Aalto University
School of Electrical Engineering
Master's Programme in Automation and Electrical Engineering

Anastasiia Kravtcova

Blood vessel detection in medical procedures using laser Doppler flowmetry

Master's Thesis
Espoo, May 11, 2017

Supervisor: Prof. Quan Zhou
Advisor: M.Sc. Harri Wijaya

Aalto University
School of Electrical Engineering
Master's Programme in Automation and Electrical Engineering

ABSTRACT OF MASTER'S THESIS

Author:	Anastasiia Kravtcova		
Title:	Blood vessel detection in medical procedures using laser Doppler flowmetry		
Date:	May 11, 2017	**Pages:**	vi + 79
Major:	Translational Engineering	**Code:**	ELEC3023
Supervisor:	Prof. Quan Zhou		
Advisor:	M.Sc. Harri Wijaya		

The needle procedures such as coronary angioplasty and coronary artery bypass graft installation are the most common surgical interventions performed in medical practice, and the accuracy of the catheter needle placement defines the success of the whole operation. Due to anatomical variations in patients, finding and puncturing the correct blood vessel is a challenging step, and the needle guidance might significantly simplify the process. Therefore, the primary aim of this work was to develop a novel blood vessel detection system based on laser Doppler flowmetry (LDF) technology that will improve the quality of medical needle procedures.

In this work, LDF measurement setup was designed, assembled and evaluated. The setup includes custom laser-detector system, two invasive measurements probes, two experimental phantoms and data acquisition software. The optical properties of human tissue and blood were examined in order to define the required laser characteristics and relevant tissue-mimicking materials. The data processing was based on the power spectrum analysis, from which the perfusion parameter was extracted. The measurement range of the system was assessed in respect to the various criteria such as penetration angle, depth and site. The applicability of LDF in the needle procedures was evaluated.

The experimental results demonstrated that the blood vessel can be successfully detected in the wide angles range and at different penetration sites. The differentiation between low and high blood flow speeds is also possible. Moreover, the potential of the measurements in tissue was demonstrated. However, certain limitations need to be addressed. It was discovered, that the distiction between the arteria and the vein is challenging, and the penetration depth inside the tissue is restricted. Nevertheless, the proposed technology can be implemented in the needle procedures and a number of other medical applications, such as laparoscopic surgeries and biopsies.

Keywords:	laser Doppler flowmetry, laser systems, medical application, medical procedure, blood vessel detection, signal processing
Language:	English

Preface

First of all, I address many thanks to my supervisor Quan Zhou for granting me a unique opportunity to work on this project. I also want to thank my advisor Harri Wijaya and everyone else from Micro- and nanorobotics research group for the comments and feedback, which helped me in progress of my work.
Furthermore, I would like to express my gratitude to people who shared their professional knowledge and expertise with me. I would like to thank Edite Figueiras for her invaluable help when nobody else could assist me. I am also grateful to Andryi Shevchenko for his guidance regarding the laser systems, and to He Yang for assistance in challenging fiber works. Moreover, I thank Visa Sippola for our fruitful conversations regarding the medical side of the work.
Finally, I forward very special thanks to my dearest Vlad for his patience and support during the last months, my big family and my best friend for their love, which I can feel even so far away.

Espoo, May 11, 2017

Anastasiia Kravtcova

Abbreviations and Acronyms

AC	Alternating current
AU	Arbitrary unit
BNC	Bayonet Neill-Concelman connector
BZ	Biological zero
CMBC	Concentration of moving blood cells
CT	Computer tomography
DAQ	Data acquisition
DC	Direct current
FDA	Food and Drug Administration
Hb SatO2 0%	Deoxygenated hemoglobin
Hb SatO2 100%	Oxygenated hemoglobin
LDF	Laser Doppler flowmetry
LDFI	Laser Doppler flowmetry imaging
MRI	Magnetic resonance tomography
NIR	Near-infrared
PD	Photodiode
Perf	Perfusion
PSD	Power spectral density
RBC	Red blood cells
Si	Silicon

Contents

Chapter 1

Introduction

Nowadays, biomedical engineering undergoes a comprehensive development due to the advancement of technology. Researchers constantly propose new technical solutions in order to improve existing medical equipment and procedures. Even minor upgrade of technology might play a significant role in the quality of treatment and care that patients receive. According to statistics, the needle procedures such as coronary angioplasty and coronary artery bypass graft installation are included into the list of the most commonly performed interventions [1]. They both involve installation of the catheter as an initial step, and the quality of action partially defines the success of the whole procedure. Thus, an enhancement of diverse medical needle procedures utilizing laser Doppler effect was a primary goal of this work.

Medical needle procedures comprise various interventions such as catheterization, needle biopsies, arterial line or epidural needle placements. In these interventions, the big blood vessels are the primary target or, in contrast, the potential hazard because puncturing might be fatal to the patient. Due to anatomical variations, the exact location of the vessel varies making the needle insertion challenging for the doctor. Consequently, the detection of the blood vessel prior to puncturing is required. Moreover, the possibility to differentiate the blood vessel type by measurements of velocity, direction or oxygenation level of the blood flow, would be a considerable advantage.

Various techniques, based on different physical phenomena, have been investigated for blood vessel detection application. To our knowledge, laser Doppler method was not used for that purpose up to now. Therefore, it was selected as a primary technology due to its uniqueness in the proposed application. Laser Doppler flowmetry (LDF) technology is conventionally used for the assessment of microcirculation meaning that it primarily targets small capillaries with negligibly low velocity of the blood flow. Consequently, the first research problem of this work is whether LDF can be utilized in

measurements of high speed and powerful flows, and whether differentiation of velocities is practically possible. The second research problem concerns the penetration ranges of the system because they define the effectiveness of LDF measurements in clinical environment. Finally, the third research problem is whether LDF measurements are reliable in tissue-mimicking phantom, which can significantly disturb the signal. Answers to these three questions will define if the proposed technique is a real enhancement of the medical needle procedures.

The aim of this work was to create a custom LDF measurement system, evaluate it and answer the above mentioned questions. This thesis is divided in six chapters. After introduction, the main technology of the work is presented in chapter 2. Chapter 3 gives an overview of the medical background relevant to this work, and reviews the optical properties of the tissue involved in LDF measurements. The design of the system, assembled setup and measurement procedures are introduced in chapter 4. The obtained results, future prospective and potential improvements are discussed in chapter 5. Finally, conclusion in chapter 6 summarizes this work.

Chapter 2

Laser Doppler flowmetry

In this work, the novel approach of blood vessel detection based on laser Doppler flowmetry technology was assessed. It is important to emphasize what are the benefits of LDF over other techniques, which can be utilized in the proposed application. Thus, such techniques and the advantages of LDF are explained in section 2.1. Further, history of LDF development is provided in section 2.2. The principles of LDF, details of signal processing and hardware overview are presented in sections 2.3 and 2.4. Finally, the limitations of LDF and available commercial products are discussed in sections 2.5 and 2.6 respectively.

2.1 Methods for blood vessel determination

Nowadays, blood vessels in human body can be distinguished and visualized using common methods such as catheter angiography and ultrasound examination. Catheter angiography technique is usually implemented in the medical procedures such as stents implantation, detection of abnormalities in arteries and aorta, narrowed blood vessels identification. It is performed by inserting the catheter into the groin, the arm or the femoral artery, with further injection of the contrast agent, which spreads with the blood flow inside the blood vessels throughout the human body [2]. Then, X-ray tomography, computer tomography (CT) or magnetic resonance tomography (MRI) are used to visualize the contrasted vessels [2]. Unfortunately, angiography cannot be useful in the initial catheter installation so it is performed without any guidance. Therefore, other methods of blood vessel and flow detection, which do not require preliminary blood flow modifications, have been developed.

The term "blood flow" is defined as a laminar stream of the blood cells. Consequently, the detection of the blood flow can be done by recognizing the presence of moving blood cells and their speed. Tanimoto et al. demonstrated how mechanical force sensors can be used for this purpose [3]. They managed to integrate the force sensor into the medical needle and show an increasing force when it comes in contact with the blood vessel. However, this method requires direct contact with the vessel, which increases the risk of puncturing the undesired one.

Further studies revealed that the Doppler effect can be effectively used to determine the flow movement. In general, the Doppler effect is a change of frequency of monochromatic wave due to its interaction with the moving object. The blood flow detection methods, which are based on the Doppler effect in different waves are described in the following sections.

2.1.1 Doppler ultrasound technique

One type of wave used with Doppler technique is mechanical ultrasound wave. Active research of using ultrasound in the blood flow detection started in the second half of the 20th century. In 1970s, Baker et al. and Sigel et al. demonstrated that the blood flow can be effectively sensed by means of the Doppler effect which ultrasound wave undergoes when interacting with the flow [4, 5]. They also discussed variations of the technique and, especially, types of ultrasound wave: continuous and pulsed [4, 5]. Besides, Sigel et al. clinically tested the proposed method proving its applicability in diagnostics of specific diseases [5].

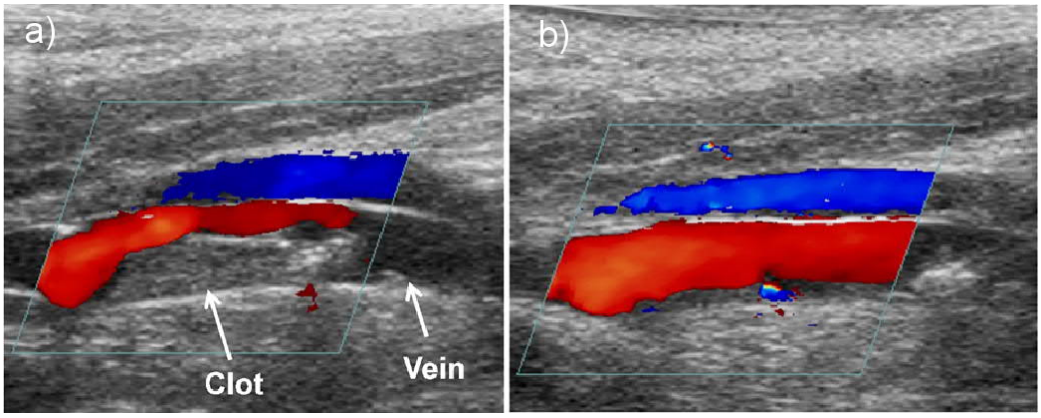

Figure 2.1: Example image of the Doppler ultrasound procedure. (a) The blood vessel is blocked by a clot. (b) Clot was removed and the blood flow restored. Adopted from [6].

Nowadays, the Doppler effect in ultrasound wave is well studied and is widely implemented in ultrasound examination that employ Doppler module combined with traditional ultrasound machine. In such configuration, doctors have an opportunity to visualize the blood vessels and the blood flow inside them. Figure 2.1 demonstrates an example of Doppler ultrasound image, where the blood vessel and the blood flow inside are visualized. In figure 2.1 (a), the flow is disturbed by the clot formed on the wall of the vessel, while in figure 2.1 (b) normal flow is restored. Such imaging is particularly important in diagnostics of blood vessels thrombosis or stenosis, when the blood flow is blocked at certain location due to physical barrier.

Another interesting and special application of ultrasound is the needle insertion procedure. In this technique, doctors use traditional ultrasound probe to visualize the blood vessel, as depicted in figure 2.2 (a). As the needle is inserted and approaches the blood vessel, it becomes observable under ultrasound beam inside the vessel (figure 2.2 (b)).

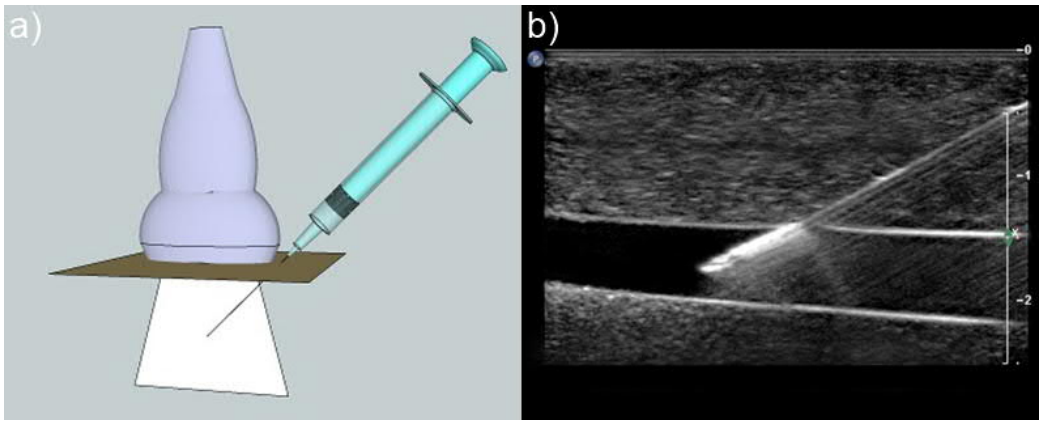

Figure 2.2: Doppler ultrasound guided needle insertion. (a) Schematic representation of the procedure when the needle, approaching the blood vessel, is visualized with ultrasound probe. (b) Real ultrasound image of the needle inserted into the blood vessel. Adopted from [7, 8].

Although conventional ultrasound as well as Doppler ultrasound were proved to be beneficial in the blood flow examination, there are significant limitations. One drawback is the size of the equipment and the need of Doppler system integration into ultrasound machine. Such setup can be bulky, hardly portable and expensive. The second drawback is the low spatial resolution of the measurements. In fact, only approximate location of the blood flow blockage or needle insertion point can be defined, which is a significant disadvantage from the treatment and intervention point of view.

2.1.2 Laser Doppler technology

Another type of wave used with the Doppler Effect is electromagnetic light wave or, in particular, the laser. Thus, the technique used for the blood flow evaluation is called laser Doppler flowmetry. The general principle of LDF is an interaction of monochromatic laser light with the living tissue and the blood vessels.

History of LDF began in the same period when Doppler ultrasound technology was proposed. In 1972, Riva et al. presented the first very simple LDF device for the blood flow measurements in rabbits [9]. Over the years, the method underwent numerous improvements such as introduction of the optical probes, implementation of semiconductor lasers instead of gas lasers, and development of new signal analysis algorithms. Although a significant progress in LDF measurements was achieved, real applications in medical

environment are still very restricted.

Nowadays, LDF technology is used in clinical practice in a very limited manner. Food and Drug Administration (FDA) approved devices only from few manufacturers, the biggest of which are Perimed Instruments and Moor Instruments (K974285 and K083082 FDA premarket submission numbers correspondingly). Both manufacturers provide blood flow monitoring equipment with different probes, which can be attached to the skin or used in invasive measurements. The signal is processed by embedded analysis unit [10, 11]. LDF proved its efficiency in assessment of such conditions as peripheral vascular disease, diabetes, amputation, plastic surgery and burns [12]. However, there are challenges in LDF measurements, which prevent the technique from being widely used. These are discussed in details in the following chapters.

Laser Doppler flowmetry technology utilizes a shift of the laser light frequency (Doppler shift), which occurs when the light is scattered by red blood cell (RBC) or by another moving particle. By analyzing the shifted frequency of backscattered light, several important parameters about RBCs can be deducted. One is the concentration (tissue fraction) of the moving blood cells (CMBC), which is the component of the second parameter called perfusion. Perfusion contains both CMBC and velocity information about the blood flow, and allows to find a relative velocity of RBC. [13] The advantages of LDF over Doppler Ultrasound are very high spatial resolution due to small measurement point and simplicity of the setup as no bulky and expensive equipment is required. On the basis of such superiority of LDF, this technology was selected as a primary in this work.

2.2 History of laser Doppler flowmetry

The development of LDF started almost fifty years ago. As was previously mentioned, the first LDF experiments were reported in 1972 by Riva et al. [9]. However, it was Stern who invented the blood perfusion measurements in 1975 [14]. He reported the possibility of distinguishing between the microvascular compartments by comparing the blood flow velocities extracted from photocurrent of the detector containing backscattered light frequency [14]. Further, Bonner and Nossal presented the first theoretical model for the Laser Doppler measurements of the blood flow in human tissue in 1981 [15]. This became the fundamental model, which is used nowadays as a basis for LDF signal processing.

During the past decades, the understanding of Laser Doppler method

was significantly broadened mostly due to the development of Monte Carlo simulations, which allowed modelling of real tissue properties and prediction of scattering events [13, 16]. Additionally, several methods for resolving relative velocity of the moving blood cells and tissue perfusion were developed [17, 18]. Furthermore, in 1980s the technology was expanded and laser Doppler flowmetry imaging (LDFI) method was developed. Significantly bigger tissue area can be measured with LDFI in comparison with one-point examination by traditional LDF [19, 20]. However, the main drawback of LDFI is decreased spatial resolution of the measurement [21]. Hence, it cannot be used in applications, where spatial precision is required.

Integrated and miniaturized laser Doppler flowmeters have been created and became the most significant and recent developments in LDF for health care industry [22, 23]. By utilizing the advantages of micromachining techniques, LDF components and signal analysis electronics are embedded into a single sensor, which can be fixed anywhere on the skin [23]. Moreover, communication between the sensor and the smartphone can be established, making the device useful in home health monitoring and continuous disease diagnostics [24].

2.3 Laser Doppler flowmetry principles and signal analysis

The Doppler effect in sound wave is a well-known phenomenon, however, its principles are different when the Doppler effect occurs in electromagnetic wave such as light. The phenomenon becomes even more complex when arises inside the human tissue, which is very heterogeneous structure. Thus, the basic Doppler theory and subsequent extension of it towards the laser-tissue interaction must be considered in order to understand LDF principles.

2.3.1 The Doppler effect

Traditional Doppler effect is easily observed in everyday life. When one walks along the street (the listener), and an ambulance with sirens (the source) passes by, human ears perceive the sound of sirens as a varying signal at different position of the vehicle, although the sound frequency stays constant. This occurs due to the fact that the listener moves with some velocity and direction, which affect the frequency that the listener percepts. [21, 25] Equation 2.1 demonstrates how this frequency (f_L) is obtained when velocities of the listener and the source are known.

$$f_L = \frac{\frac{C \cdot T}{\lambda} \pm \frac{V_L \cdot T}{\lambda}}{T} = \frac{C \pm V_L}{\lambda} = \frac{C \pm V_L}{\frac{C}{f_S}} = f_S \cdot (1 \pm \frac{V_L}{C}), \tag{2.1}$$

where f_L is the frequency experienced by the listener, C and V_L denote the speed of wave from the source and the speed of the listener respectively, λ is the wavelength of the original wave, and T is a time unit per which f_L is calculated [25]. Sign $\pm$ denotes the movement direction of the listener.

Frequency (Doppler) shift, f_D, is defined as a difference between the frequency experienced by the listener, f_L, and the one produced by the source, f_S, as shown in equation 2.2.

$$f_D = f_L - f_S = f_S \cdot (1 \pm \frac{V_L}{C}) - f_S = \frac{V_L \cdot f_S}{C}. \tag{2.2}$$

According to equation 2.2, the speed of the moving object should be significant in order to induce discernible f_D. The Doppler shift in sound waves is easily observable at low frequencies of 20 Hz to 20 kHz (audible range), and up to 1 MHz (ultrasound). In contrast, the Doppler shift that results from collision of the laser wave with the moving particles is very small in comparison to the incident frequency of the laser, which in THz range. Thus, the laser Doppler phenomenon is much more difficult to identify although possible due to spectral purity and high coherence of the laser light. In order to recognize it, interaction between the laser light and the moving blood particles has to be thoroughly considered. [25]

2.3.2 Single laser Doppler shift

Laser light scattering phenomena is widely used in bulk matter properties characterization such as spectroscopy. Indeed, the measurements that are performed in clear and near-uniform medium such as air or water are easy to analyze because a sample under study is the only source of the light scattering. However, various scattering sources are present when measurements are done in highly heterogeneous medium. The light that is scattered from such structures interferes with the light scattered from the object of interest, which makes measurements analysis complicated. An example of highly heterogeneous and complicated structure is human skin. Consequently, interaction of the laser light with the blood cells located inside the tissue is not straightforward.

Bonner and Nossal were the first to formulate a theoretical model of Laser Doppler blood flow measurements in human tissue [15]. They claimed that due to complex tissue matrix and optical structure, it is impossible

to uniquely predict the behavior of the light before and after interaction with the blood vessels. The reason is that initially coherent laser light is randomized by single or multiple collisions with the static tissue becoming non-coherent when incident to the moving blood cells. Randomized photons are scattered by the moving cells in various directions towards the photodetector. Photons can be scattered even more than once resulting in multiple scattering. However, modeling of such case is difficult due to extreme complexity and randomness of the events. Consequently, the simplest case of predominating single scattering is always considered when examining Laser Doppler phenomenon.

The fundamental rule behind the Doppler event is that the frequency of light, scattered by the moving object, is shifted. The shift depends on the movement of involved object and the incident photon direction. [26] Further, a single scattering event is considered in more details.

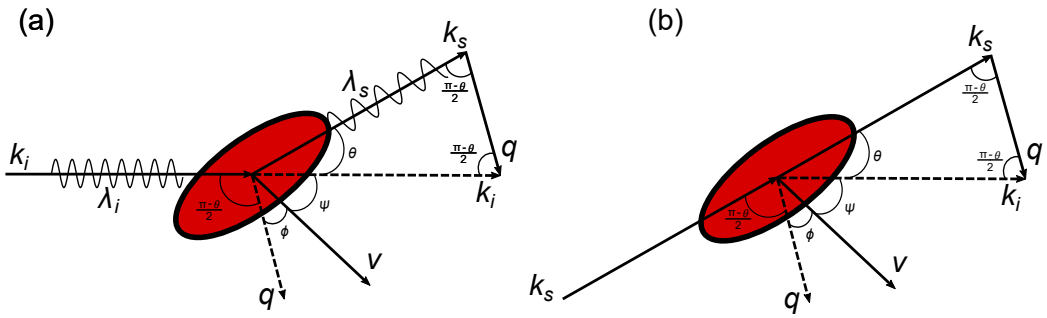

Figure 2.3: Vectors of the photon and the blood cell before and after interaction. Red object resembles a red blood cell. Vectors are defined as follows: k_i - incident vector of the photon, k_s - propagation vector of the photon after scattering, v - velocity vector of the moving object, q - difference between k_i and k_s. Angles: ψ - between V and k_i, θ - between k_i and k_s, ϕ - between q and V.

In figure 2.3, k_i describes the incident vector of the photon before interaction with the moving object, while propagation vector after scattering is k_s [27]. Velocity vector of the moving object is v, and q is the difference between incident (k_i) and scattering (k_s) vectors. The angle between V and k_i is ψ, between k_i and k_s is θ, and between q and V - ϕ.

The light incident to the moving particle has a frequency f_i. Its wavelength is defined as $\lambda = C/f_i$ (figure 2.3 (a)), where $C = C_0/n$ is the speed of light in the tissue with refractive index n where light propagates. Let us consider the time period Δt, during which the incident wave travels towards

the moving particle and hits it. The distance, which the wave accomplishes, is increased by the movement of the particle during Δt, and it is defined as:

$$\lambda_i + \Delta t \cdot V \cdot \cos\psi = \Delta t \cdot C. \tag{2.3}$$

Similarly, the distance that the scattered wave passes is obtained assuming that it has wavelength λ_s:

$$\lambda_s + \Delta t \cdot V \cdot \cos(\psi + \theta) = \Delta t \cdot C. \tag{2.4}$$

Combining equations 2.3 and 2.4, wavelength of the scattered wave λ_s is deducted:

$$\lambda_s = \frac{(\lambda_i - \lambda_i \cdot \frac{V}{C} \cdot \cos(\psi + \theta))}{(1 - \frac{V}{C} \cdot \cos(\psi))}. \tag{2.5}$$

Doppler frequency is the difference between incident and scattered frequencies:

$$f_D = f_i - f_s = C \cdot (\frac{1}{\lambda_i} - \frac{1}{\lambda_s}) = \frac{C}{\lambda_i} \cdot (\frac{1 - \frac{V}{C} \cdot \cos(\psi + \theta)}{1 - \frac{V}{C} \cdot \cos(\psi)} - 1). \tag{2.6}$$

Assuming that $V << C$, nominator in equation 2.6 is omitted giving f_D as:

$$f_D \approx \frac{V}{\lambda_i} \cdot (\cos(\psi) + \cos(\psi + \theta)). \tag{2.7}$$

Because $V << C$, incident and scattering vectors, as well as angles between k_s and q, k_i and q, can be considered equal (figure 2.3 (b)). Thus, angles between k_i and k_s are defined as:

$$\psi + \theta + \phi + \frac{(\pi - \theta)}{2} \approx \pi. \tag{2.8}$$

Then Doppler frequency from equation 2.7 can be rewritten as:

$$f_D \approx -2 \cdot \frac{V}{\lambda_i} \cdot \sin(\frac{\theta}{2}) \cdot \cos(\phi). \tag{2.9}$$

From equation 2.9 it is clear that the size of the Doppler shift depends on velocity V. Besides, the maximum Doppler shift f_D is achieved when $\sin(\theta/2)$ is maximized, as when $\theta = \pi$, which is a full backscattering condition. However, due to high anisotropy of RBCs (presented in the following chapter), forward scattering of the photons prevails in the interaction of light

with RBCs, meaning that θ is close to zero [13]. When $\theta = 0$, scattering vector q is orthogonal to the incident light vector k_i. Consequently, maximum Doppler shift is achieved when light direction is orthogonal to the moving RBCs, and thus $\cos(\phi) = 1$ [13]. This aspect must be considered when designing experimental probe and measurement setup for LDF measurements.

2.3.3 Power spectrum analysis and blood flow properties

When penetrating highly heterogeneous human tissue, the laser light undergoes scattering after interaction with the moving blood cells and the static tissue parts as figure 2.4 demonstrates. Frequency shift occurs when light scatters from the RBCs, while scattering from the static tissue does not lead to the frequency shift. In the detector, shifted and non-shifted signals are mixed resulting in varying beating frequency, which causes intensity fluctuations of the detected photocurrent. By analyzing such photocurrent, information about the RBCs flow can be deducted. [13]

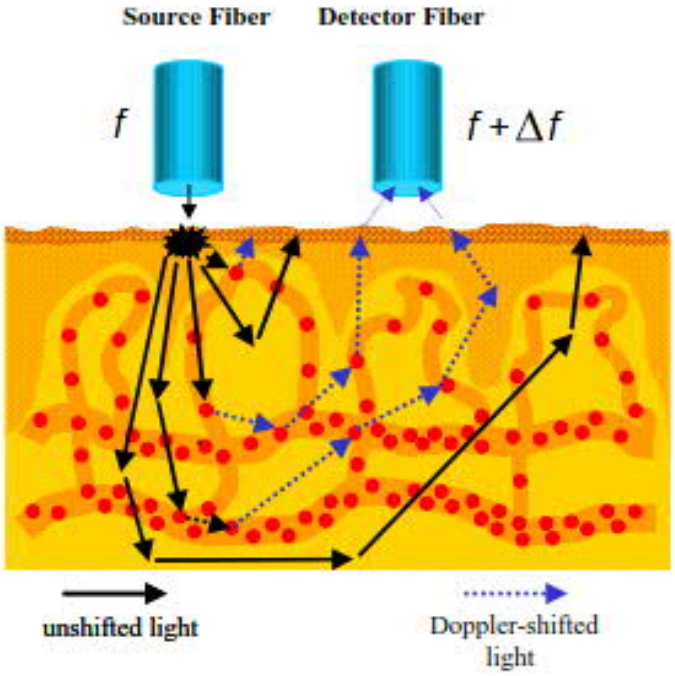

Figure 2.4: Schematic diagram of the Laser Doppler measurement. The source fiber delivers incident light to the tissue, the detector fiber collects scattered light with the beating frequency (mixture of shifted and not shifted frequency) and guides it to the detector. Adopted from [28].

Theoretical derivation of the Doppler power spectrum begins with the analysis of the photodetector response induced by the action of incident laser light. Both shifted and non-shifted light interfere on the detector forming a speckle pattern. Static frequency of the light results in the static speckle, while varying frequency induces speckle fluctuations. The varying current $i(t)$, generated in the photodetector, contains static part i_{DC} as well as time varying part i_{AC}. Static part is calculated as

$$i_{DC} = \int I(f)df, \tag{2.10}$$

where $I(f)$ is the optical Doppler spectrum in frequency domain. [26, 29]

The Doppler power spectrum represents the power spectral density (PSD) of time varying part i_{AC} of the detector current, and it is obtained as an autocorrelation function of the optical Doppler spectrum $I(f)$ as follows [26, 29]:

$$P(f) = PSD(i_{AC}) = 2(I * *I)(f), \tag{2.11}$$

where $**$ denotes the autocorrelation and $f > 0$.

The Doppler power spectrum $P(f)$ is affected by the tissue fraction of RCBs and by their speed. Fredriksson demonstrated Monte Carlo simulation, which clearly illustrates this dependence [13]. Increased speed of RBCs leads to the multiple scattering and, consequently, to the spectrum broadening (figure 2.5 (b)). This is because RBCs undergo not only higher Doppler shift on average, but also mixing of the shifts from several scattering events with different moving RBCs occurs in the detector. In contrast, higher RBCs tissue fraction, affects only the magnitude of the spectrum, which rises over the whole frequency range (figure 2.5 (a)). In this case, more photons are shifted due to increased number of RBCs leading to higher intensity of the detected signal, but the size of the Doppler shift does not change. [13, 29]

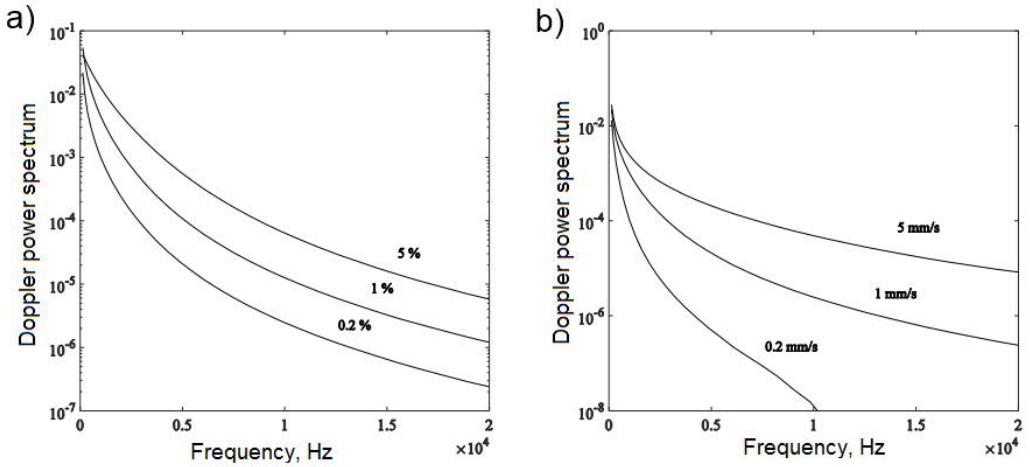

Figure 2.5: Relationship between the Doppler power spectrum and the RCBs tissue fraction or the speed obtained by Monte Carlo simulation. Frequency denotes the size of frequency shift, while Doppler power spectrum stands for the magnitude of the spectra. (a) Increased RBCs tissue fraction results in increased magnitude of the power spectrum. (b) Increased velocity leads to spectral broadening. Adopted from [29].

The general analytic correlation is that the blood flow properties are directly related to the power spectrum $P(f)$ obtained from the photodetector output signal [15]. The properties can be estimated by considering different moments of the spectrum:

$$M_i = \int f^i P(f) d(f). \tag{2.12}$$

Three parameters can be determined from the power spectrum analysis. The first parameter is concentration of moving blood cells (CMBC), which represents the fraction of RBCs in examined tissue volume. CMBC is found by calculating the power spectrum at zero moment [15]:

$$CMBC \propto M_0 \approx \int P(f) d(f). \tag{2.13}$$

The second parameter of the blood flow is perfusion (Perf). Perf is determined from the spectrum at the first moment [15]:

$$Perf \propto M_1 \approx CMBC \cdot \langle V \rangle \approx \int f P(f) d(f), \tag{2.14}$$

where $\langle V \rangle$ is the mean velocity of the blood cells, or the third parameter, which is theoretically derived by dividing the first by zero moments of the power spectrum:

$$\frac{M_1}{M_0} = \langle V \rangle . \tag{2.15}$$

Proportionality of measured perfusion and CMBC presented in equations 2.13 and 2.14 is fulfilled for low concentrations of the moving particles, or if the number of multiple collisions is low. This condition is achieved in microcirculation measurements when non-invasive probe is placed on the skin, and the underneath blood flow in small capillaries is examined. In contrast, if concentration of the RBCs is high, Perf and CMBC vary non-linearly (figures 2.6 (a) and (b)) as when the blood flow is measured with the invasive probe in direct contact with the blood vessel. Moreover, theoretical model of LDF microcirculation measurements states that measured perfusion is proportional to the flow velocity regardless of the flow concentration providing the real concentration of the measured solution is constant (figure 2.6 (c)). [15, 26] However, experimental studies demonstrate deviation from this model.

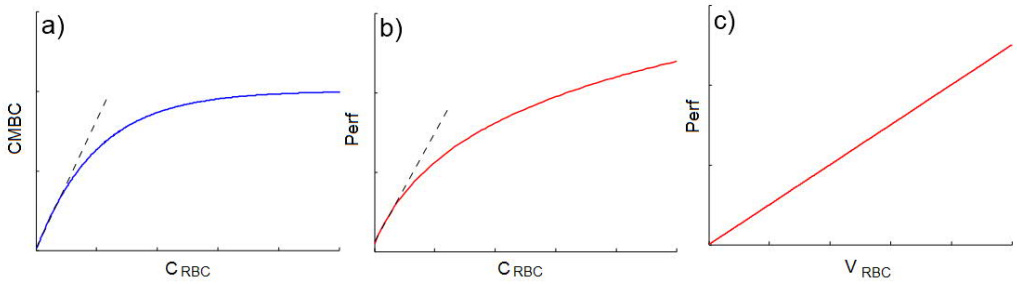

Figure 2.6: Relationship of major parameters in LDF microcirculation measurements obtained by Monte Carlo simulation. CMBC and Perf denote measured concentration of RBCs and perfusion respectively, while C_{RBC} stands for actual RBCs tissue fraction. (a) Measured CMBC and real concentration of the moving flow are linear only at low concentrations. (b) Measured Perf and real concentration of the moving flow are linear only at low concentrations. (c) Measured Perf and real velocity of the moving flow are linear independent of concentration. Adopted from [26].

Apparently, the number of multiple collisions of the photon with moving RBCs, along with RBCs concentration, define the quality of perfusion measurement. It was discussed that if photon scatters from several moving RBCs, non-linearity of perfusion estimations is observed due to alternations in the Doppler shifts directions. In practice, this results in narrowing of the power spectrum with increasing flow velocity while widening is normally expected. [30] Such deviation from theoretical model makes determination of the high-speed blood flow challenging and ambiguous.

Special methods for LDF data processing have been developed [17, 31]. Unfortunately, none of them can be used to absolutely distinguish the velocity of the flow, but they provide relative information about the flow speed variations. Nilsson was the first who proposed a method for calculating perfusion value from the real measurement data [31]. The approach became traditional for LDF measurements, and it is implemented nowadays in commercial Laser Doppler Flowmeters [13]. The method includes removal of the signal noise, extraction of alternating current (AC) part of the signal, frequency weighting of the power spectrum and normalization of the signal with direct current (DC) current mean value [13]. Equation 2.16 demonstrates the perfusion calculation:

$$Perf = \frac{ACP - N}{DC^x}, \tag{2.16}$$

where DC is the mean DC part of the signal and x can be 1 or 2. N

represents the instrument noise, and ACP is AC part of the signal found as [18]:

$$ACP = \int_{l}^{h} f P_{AC}(f) d(f), \tag{2.17}$$

where l and h denote low and high cutoff frequencies respectively, and $P_{AC}(f)$ is the power spectrum of AC part of the signal.

Frequencies of the bandpass filter are usually selected as 10 Hz to 20 Hz for the lower, and as 20 kHz to 30 kHz for the higher cutoff limits. The noise coming from the tissue and the fiber movements is eliminated by the lower limit, while expected RBCs velocity defines the higher limit. Thereby, measurements with 808 nm laser wavelength and up to 10 mm/s velocity of the blood cells can be conducted in a proposed frequency range (10 Hz - 30 kHz) without losing meaningful data [28].

The parameters of instrumental noise N are usually estimated experimentally during the laser Doppler Flowmeter calibration before the actual measurements. This is done by measuring the signal at different DC levels from static scattering object, such as white plastic [13]. It is assumed that the noise contains variation in photoelectron emission rate (m), which is linear to DC part of the signal, and constant thermal noise (b) if the temperature is kept stable [13]. Consequently, instrumental noise parameters m and b are obtained by collecting several mean DC values of the signal, calculating corresponding signal power spectrum P_{noise}, and building the first polynomial of them [32, 33]:

$$P_{noise} = m \cdot DC + b, \tag{2.18}$$

where m is the slope of the first polynomial curve, b is y-axis intersection value and DC is the mean photodetector signal. Knowing parameters m and b, the noise level during the actual measurement can be calculated at certain DC value, and must be further subtracted from the measured perfusion values [34].

DC part of the signal for final measurement normalization is obtained by applying a low pass filter on the acquired data. Nilsson proposed a low cutoff frequency of 32 Hz, however, 0.5 Hz and 25 Hz cutoff values were used in other experimental research depending on the level of the setup noise [35, 36]. Normalization of the signal with DC current mean value DC, or its squared value DC^2, allows elimination of DC fluctuation and employing AC component of the signal in the final perfusion calculation [13].

2.4 Hardware considerations for laser Doppler flowmetry

Successful LDF measurement is a combination of well-established hardware setup and well-planned signal acquisition. Both parts have important aspects, which must be taken into account in order to get a signal that is sufficient for analysis and contains necessary information. Expected Doppler shift calculation before LDF measurement plays a crucial role in high quality signal record, while measurement probe design affects the number of collected Doppler shifted photons, and thus measurement depth. Quality of the recorded data defines if the meaningful information about measured flow can be deducted. Measurement depth determines the examined tissue volume.

2.4.1 Estimation of the Doppler shift and signal acquisition

A suitable sampling frequency for LDF signal acquisition is determined by estimating the maximum value of the Doppler shift. Assumption for ideal estimation is that no multiple shifts occur during the experiment. Theoretical model of the laser interaction with a single RBC, described in the previous sections, is used for expected shift calculation, as was demonstrated by Boggett et al. [37]:

$$f_D = \frac{\pm 2 \cdot V}{\lambda}, \tag{2.19}$$

where λ is the wavelength of the incident light, V is the velocity of the blood cells, $\pm$ sign defines the direction of the moving flow. The angles between incident and scattered light vectors and between their difference and RBC velocity vectors are not included into this estimation leading to calculation of the maximum possible Doppler shift value.

According to equation 2.19, f_D varies with the speed of the blood flow, and with the wavelength of incident light. For example, if the wavelength of the laser is 808 nm, and the flow inside venules is 4 mm/s, expected Doppler shift is approximately 10 kHz. According to that calculation, necessary sampling frequency can be selected, which is discussed in the following section. Similarly, fixed laser wavelength or restricted hardware sampling frequency can be used for calculation of the maximum observable velocity of the flow. If sampling frequency of the acquisition is too small for selected flow velocity, acquired data will not contain reliable information about the flow under study.

In order to select a suitable sampling frequency for a certain LDF measurement, the sampling frequency of data acquisition device must follow Nyquist sampling theorem. It states that in order to avoid measurement errors and aliasing, the rate of acquisition must be at least two times higher than the highest expected frequency of the signal [38]. Consequently, if expected Doppler shift (calculated by equation 2.19) is 10 kHz, then the sampling rate of the signal acquisition must be at least 20 kHz. However, it is important to understand that multiple shifted photons have much bigger frequency shift that single shifted ones. Consequently, they are collected if unnecessarily high sampling frequency is used. Only the single shifted photons carry meaningful information about the flow. Thus, the data that is acquired at the sampling rate much higher than is derived by Nyquist theorem might be unreliable.

2.4.2 Setup based on the fiber optics probe

The most widely used setup for LDF measurements utilizes the fiber optics probe. One fiber delivers incident laser light to the tissue, while the second fiber collects scattered light and delivers it to the detector. In the tissue, the laser light undergoes several events. One part of it passes through the tissue and is not collected by the detector. Some light is reflected by the static tissue without the frequency shift. The last part of the light interacts with the moving blood cells and it is frequency shifted. The latter two light portions are mixed when collected by the detector.

Fibers separation is the distance between the source and the detector fibers. It defines the penetration depth of the measurement. Scattered photons from the deeper tissue area are collected with bigger fiber separation as figure 2.7 indicates [39–41].

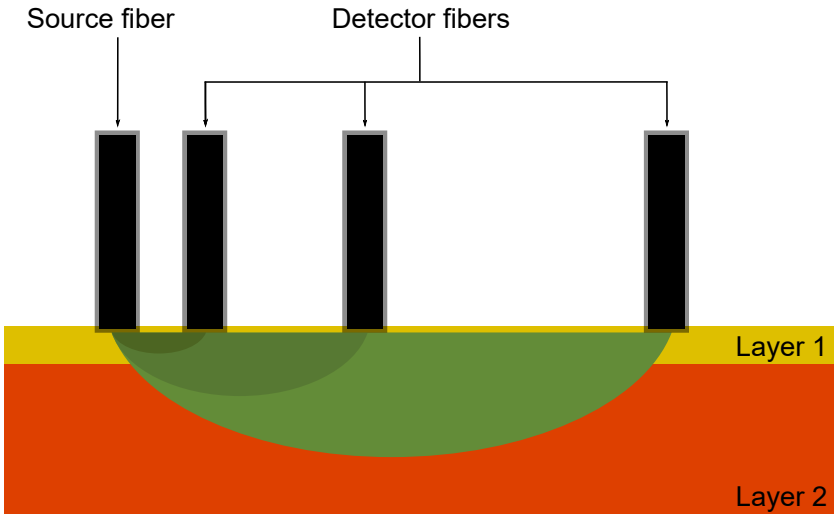

Figure 2.7: Relation between fibers separation and penetration depth. Increased separation leads to deeper measurement possibility. Layers 1 and 2 are the abstract layers of examined tissue.

Fibers separation value does not have any conventional limit. However, it is important to understand that bigger separation and subsequent deeper penetration increase the chances of photon interaction with several blood vessels resulting in multiple scattering and non-linear estimations of CMBC and Perf parameters. The most widely used commercial probes from Perimed utilize fiber separation of 0.4 mm to 1.2 mm [42]. Very few researches succeeded in using bigger fiber separation. For instance, Kolkman et al. demonstrated measurement results for up to 4 mm fiber spacing in increased depth LDF measurements [40, 43].

2.4.3 Laser source and photodetector selection

The first Laser Doppler flowmeters used gas lasers, particularly HeNe lasers with the wavelength of 632.8 nm. With the development of semiconductor industry, gas lasers were replaced by the laser diodes (LD). The main advantages of LDs are smaller size and price, lower power consumption and possibility to modulate the light wave (continuous wave or pulsed wave). However, LDs have certain limitations, one of which is broader emission spectrum in comparison with gas lasers, which leads to small coherence length and introduces additional problems to the signal analysis. Another limitation is operating wavelength and output power dependence on the working temperature. Operating current induces temperature rise, which usually leads to

unstable wavelength and increased output power. However, the effects of the mentioned drawbacks can be minimized by proper temperature control during LD operation in conjunction with selection of LD with narrow emission spectrum. [27]

The wavelength of LD is selected according to the optical properties of the tissue under LDF measurement. The primary target of LDF is the blood, which determines suitable wavelength in the first place. Nevertheless, all tissue components and their optical properties must be considered in order to select correct laser wavelength. The optical properties relevant for this work are described in the following chapter. Classic wavelength range for LDF applications is from 600 nm to 1000 nm. [27]

Penetration depth is also affected by the wavelength of the laser. The photons with longer wavelength penetrate deeper in the tissue than the photons that have shorter wavelength. Thus, bigger sampling volume can be achieved. [27] Another parameter, which somehow affects the penetration depth, is the power of the laser. Conventionally, the power of 1 mW to 5 mW is used, which is mostly defined by safety regulations declared by NEN-EN 60825:1994 standard (International Electrotechnical Commission, Geneva, Switzerland). However, experimental studies with higher power up to 120 mW demonstrated deeper light penetration although the power is above the approved level [44].

Traditionally, backscattered photons are registered by photodetector, which is based on the photo diode (PD). Silicon (Si) PD is suitable for LDs with the wavelengths ranging from 600 nm to 1000 nm due to spectral range from visible to near-infrared (NIR) light. The PDs operate in an electronic circuit, which is built according to the requirements of particular application. The most basic circuit transforms generated photocurrent into voltage with or without bias [45]. In applications where amplification of the signal is necessary, as in LDF measurements, the PD is used with operational amplifier circuit [45]. On the market, commercial photodetectors with built-in amplifiers are available.

2.5 Limitations of laser Doppler flowmetry technology

Since certain challenges of LDF cannot be predicted or simulated, they may lead to the measurement errors. Although vast research has been done in order to improve LDF measurements quality, the measurement results are still more relative than absolute.

The first challenge is multiple scattering of the laser photons [13]. Theoretical model of Bonner and Nossal was developed for microcirculation estimation based on the assumption that single scattering dominates in LDF measurements. However, later research demonstrated that multiple scattering occurs with higher probability. Thus, conventional perfusion estimation is not accurate and usually non-linear at high concentrations and velocities of RBCs. Several algorithms were developed in order to compensate for multiple scattering, but it is not possible to prove their efficiency due to complicated and uncertain modelling of the scattering phenomena.

Another limitation of LDF comes from the motion artefacts. The movement of both the tissue and the fiber leads to intensity fluctuations on the detector and, thus, output errors. The amplitude of these fluctuations might be larger than the actual Doppler signal meaning that measurements cannot be successful [13, 27]. Natural movement of the living tissue, such as breathing and blood vessels expansion due to pressurize flow, cannot be controlled or eliminated. However, it is possible to manage fibers movements if properly constructed probes are utilized.

One more challenge behind LDF measurements is biological zero (BZ). This condition occurs during blood vessel occlusion, when the blood cells do not move but experience the Brownian motion, which is conventionally considered as BZ. BZ is the main reason why perfusion value never reaches zero even if the blood flow is definitely arrested. [13, 27] It is argued whether BZ should be recorded separately and then subtracted from measurement signal, because similarity of RBCs behavior in arrested and moving blood flow has not yet been assessed [27].

There are also limitations of LDF that arise from the examined tissue. Due to small measurement volume, it is nearly impossible to place the probe to the identical location in different measurements [46]. This aspect leads to poor reproducibility of LDF measurements. The tissue is a very heterogeneous structure, and constituting tissue parts have different optical properties. Besides, blood circulation varies over time depending on the heart rate, the blood pressure and other physiological factors. Combination of the tissue and blood features result in fluctuation of the photon path lengths

and inaccurate detection. Moreover, the lack of quantitative units makes the comparison of measurement results inexpedient because it is hard to predict or estimate the measurement volume and exact tissue components and properties. For this reason, perfusion measurements are presented in arbitrary units (AU).

2.6 Commercial laser Doppler flowmeters

As was mentioned in section 2.1.2, only two LDF technology manufacturers have been approved by FDA and can be implemented in clinical environment. The first one in Perimed AB, Sweden. Perimed have developed diverse equipment for evaluation of the blood flow properties. One device is PeriFlux System 5000, which is Laser Doppler Perfusion Monitor. It is capable of measuring local microvascular perfusion including capillaries, arterioles and venules [10]. Figure 2.8 demonstrates PeriFlux System 5000 and examples of the probe installation.

Figure 2.8: PeriFlux System 5000 device (on the left) and example of the skin measurement probes installation (on the right). Reprinted from [10].

PeriFlux 5000 uses 780 nm wavelength 1 mW power laser [13]. Device is connected to the computer or laptop for continuous output monitoring. Various probes are utilized with PeriFlux in LDF measurements. Skin probes (in figure 2.8) are fixed on the skin by means of tape or sutures for rigid contact [10]. Invasive probes are used in acute invasive measurements in organs and tissues [10]. Many researchers have used Perimed instruments as a reference for their measurements [36], or as a signal processing tool when custom systems were not created [13, 47].

Moor Instruments Ltd. is another FDA approved supplier of Laser Doppler Monitors, which manufactures MoorVMS-LDF device (figure 2.9). The operation principle is similar to PeriFlux 5000. Microcirculatory blood flow monitoring is the primary target of the device.

Figure 2.9: MoorVMS-LDF device from Moor Instruments, and three compatible probes. Reprinted from [11].

The main difference of MoorVMS-LDF from PeriFlux 5000 is the laser. It implements 785 nm wavelength 2.5 mW power laser diode [11]. In terms of applications, probes and signal monitoring MoorVMS-LDF and PeriFlux 5000 provide similar capabilities. Both devices clearly showed the possibility to evaluate the microcirculation in the tissue. However, neither demonstrated the possibility of large blood vessel detection in applications with the needles, which is of an interest in this work.

Chapter 3

Principles of light behavior in tissue

In this chapter, light behaviour in human tissue is described. First, relevant medical background including anatomy and the properties of the tissue, the blood and the blood vessels are explained in section 3.1. Then, the optical properties of every tissue component are clarified in section 3.2. Based on that, laser wavelength range selection is explained in the last section 3.3.

3.1 Medical background

Laser Doppler flowmetry measurement results are strongly dependent on the assumptions regarding the blood flow characteristics and optical parameters of the tissue. Moreover, the design of the proper evaluation experiments must be based on the real tissue properties. Consequently, it is important to define relevant features of the tissue in order to configure suitable hardware, data acquisition and signal processing specifications.

The femoral, the groin and the arm arteries are the most frequently catheterized arteries in the medical needle procedures. They are located directly under the skin and fat layer and above the muscles at the puncture site. Thus, the light propagates through the skin and fat at most before reaching the blood vessel. Furthermore, light interaction with the blood vessel wall takes place. Thus, properties of the blood, skin and the blood vessels have been studied. Parameters relevant to the topic are described in the following sections.

3.1.1 Human skin structure

Human skin consists of two layers: epidermis and dermis. Additionally, a variable amount of fat tissue is located underneath the dermis. Figure 3.1 demonstrates the structure of the skin.

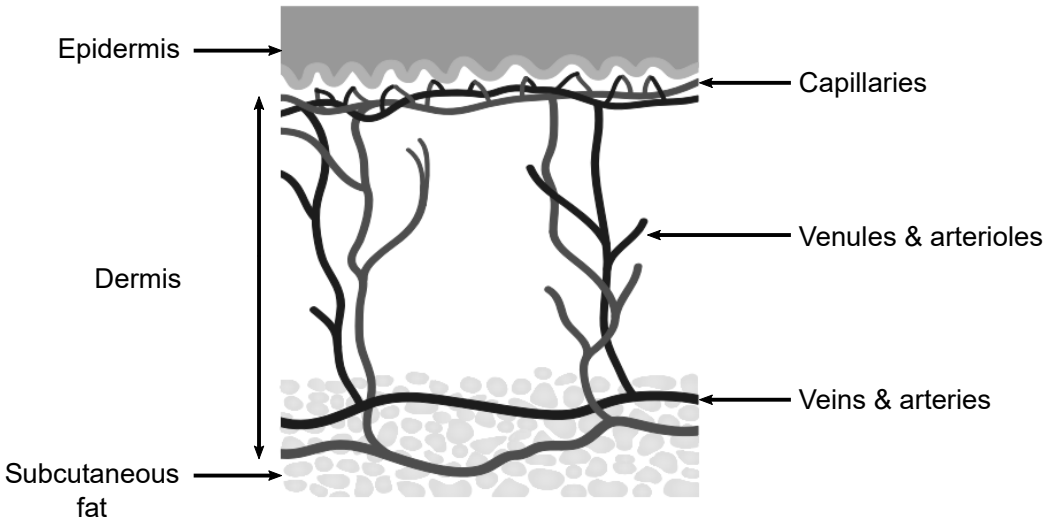

Figure 3.1: Structure of the skin presented by epidermis, dermis, subcutaneous fat, and blood vessels. Three types of blood vessels grouped by the size are located at different depths in dermis. Adopted from [29].

The top layer of the skin is epidermis that is presented by keratinized stratified squamous epithelium [48]. Its surface mostly consists of dead cells and generally lacks blood vessels. Epithelium contains skin pigment called melanin, which is responsible for skin color of different tone and tan. The amount of melanin varies in different places on the body. Synthesis of melanin can be stimulated by ultraviolet radiation resulting in increased pigment concentration.

The second layer of the skin below epidermis is called dermis [48]. Dermis is mostly composed of collagen, but also contains blood vessels in contrast to epidermis. Some parts of the skin, where dermis is thin and capillaries are close to the skin surface, may have red colors instead of brown defined by melanin. Red color originates from the red pigment present in the blood called hemoglobin that is described in the next section.

The last skin structure to be considered is subcutaneous fat. It is located under the dermis and is composed of lipid cells [48, 49] . Thickness of subcutaneous fat layer varies. If the person is obese, subcutaneous fat volume

is bigger, while infants and elderly people have less fat under dermis.

3.1.2 Blood properties

Human blood is presented by plasma and several types of cells: erythrocytes, leukocytes and thrombocytes. Plasma mostly consists of water (92%) and the rest are proteins and nutrients in small fractions. On average, 54% of blood volume is plasma. Only around 1% of blood volume is presented by leukocytes and thrombocytes. Consequently, near 45% of the whole blood are erythrocytes, which are the red blood cells. RBCs have a normal size of 6 µm to 8 µm.

Hemoglobin is a protein of erythrocyte, a red blood cell, which carries the oxygen throughout the human body [50]. It can be in a form of oxyhemoglobin or deoxyhemoglobin defined by the oxygen content. In the first form, it carries oxygen from lungs to the organs, while in the second form, no oxygen is attached to deoxyhemoglobin, but it is CO_2 that binds to it to be removed through the lungs.

3.1.3 Blood vessels types and structure

The blood vessel is an essential part of circulatory system that transports blood in the human body. There are three main types of blood vessels: arteries, capillaries and veins. The blood flow characteristics of each blood vessel type are defined by the purpose of the flow.

The strongest blood vessel type is called artery. It carries blood from the heart under the high pressure generated by ventricular systole. Pressurized blood flow in arteries has the highest speed among all blood vessels. Capillaries have different role in circulatory system. Body materials, such as water, oxygen and nutrients, are exchanged between the blood and the tissue fluid through one cell thick and highly permeable walls of capillaries. The blood flow travels from arteries to capillaries through the intensive branching of arterioles, which defines low flow speed in capillaries. The blood circulation in capillaries is always referred to as microcirculation. The third type of the blood vessels is called vein. Veins collect the blood from capillaries through venules, and transfer it towards the heart. The pressure does not affect venous blood flow as it depends on skeletal muscles massaging functions and the presence of one-way venous valves. Consequently, the blood speed in veins is lower than in arteries. [48] Table 3.1 summarizes main blood vessels types, their typical diameters and the blood flow speeds.

Table 3.1: The main blood vessel types and corresponding blood flow speeds. Adopted from [48].

Blood vessel type	Flow speed	Diameter
Arteries and aorta	400 - 1200 mm/s	Up to 2.5 cm
Arterioles	Up to 15 mm/s	20 - 50 µm
Veins and venae cavae	80 - 150 mm/s	Up to 3 cm
Venules	Up to 5 mm/s	20 µm
Capillaries	0.3 - 0.4 mm/s	5 - 9 µm

It is clear from table 3.1 that the blood flow speeds in different blood vessels vary significantly with up to 1000 times difference. The understanding of such diversity is important for estimation of the measurement limitations. Moreover, variation of diameters dramatically affects the sampling volume and the blood tissue fraction during the measurements.

The walls of the big blood vessels are primarily presented by elastin fibers, endothelial cells and smooth muscles, which are distributed in three layers [51]. Arteries have more muscles than veins because the arterial blood flow is more powerful and higher elasticity of the vessel wall is required. Capillaries, in contrast, do not carry pressurized blood flow and their walls are built from one single layer of endothelial cells.

3.2 Optical properties of the tissue

The human tissue, as was described above, is a heterogeneous structure. It consists of two different skin layers, water and the blood vessels, all of which influence the light. In order to understand the processes that occur when the laser light penetrates the tissue, a study of the optical properties was conducted.

The complex structure of the human tissue and its effect on absorption and scattering of the light radiation was thoroughly discussed by Tuchin et al. [52, 53]. Average refractive index of biological tissue is higher than that of the air. Consequently, the collimated laser light diffuses and undergoes two processes: reflection and penetration. Penetration occurs in two ways. Some light, depending on the wavelength, is absorbed, and some is scattered. Due to backscattering, the intensity of reflected radiation reaches 70% comparing to the incident light, which allows the analysis of reflected light and further diagnostics.

Scattering and absorption properties and corresponding coefficients are typically compared in order to correlate the optical properties of different tissue structures. Absorption is an energy loss, which light experiences when passes through any biological structure [52]. Absorbed light energy transfers into heat, participates in photochemical reactions or emits as luminescence [52]. This portion of light is never collected and does not contribute to the measured signal. Scattering is a deflection of light from its original path due to some obstacle, which blocks the light [29]. The degree of scattering depends on the incident wavelength of the light, the size of the obstacle and the mismatch of the refracting indices [29, 53].

Efficiency of absorption and scattering is given as absorption and scattering coefficients (μs and μa). Scattering coefficient μs is mostly used to characterize isotropic scattering, which is equal in all directions. However, in some structures scattering is anisotropic, or forward. That is defined by anisotropy factor g of the structure, which is the mean cosine of the scattering angle. If it is close to 0, isotropic event is expected, while value close to 1 means anisotropic scattering. The combination of anisotropy factor and scattering coefficient results in reduced scattering coefficient $\mu s'$ calculated as:

$$\mu s' = (1 - g) \cdot \mu s \tag{3.1}$$

Due to high anisotropy of biological tissues (0.85 for tissues and 0.991 for blood at 780 nm), $\mu s'$ is usually used for the optical properties assessment instead of μs [13].

When the laser irradiates any part of the skin, it affects at least two layers: epidermis and dermis. As was discussed in the previous sections, the dermis comprises blood vessels with moving blood cells and water. Also, the epidermis is presented by static cells, and subcutaneous fat is located beneath the dermis. Moreover, further interaction of the light with the wall of the blood vessel affects light propagation. Such heterogeneous tissue structure defines its varying optical properties, which must be considered in order to select the laser wavelength suitable for LDF measurements. Absorption and reduced scattering are considered in this work because they have the biggest influence on the light behavior in the laser Doppler phenomenon. Corresponding coefficients for each tissue part are summarized in tables 3.2 - 3.5 for wavelength range of 600 nm to 900 nm.

The epidermis contains no blood, and the main absorber is the color pigment melanin [54]. However, the effect of melanin is more significant at lower wavelengths, and it is not high at the considered rage. The scattering of the light occurs mostly from packed keratinized dead cells, although melanin

plays role in scattering as well [55, 56]. According to Salomatina et al., absorption and reduced scattering coefficients of epidermis are defined as in the table 3.2 [55].

Table 3.2: Absorption and reduced scattering coefficients of human skin epidermis. Data gathered from [55].

Wavelength, nm	Absorption,μa (mm$^-$1)	Scattering,μs (mm$^-$1)
600	0.4	4.2
700	0.3	3
800	0.2	2.5
900	0.08	2.2

In dermis, the optical properties are defined by the light interaction with water, collagen fibers and the blood vessels (presented in table 3.3). According to Fredriksson, water is a weak absorber in the wavelength range of 600 nm to 900 nm [57]. Moreover, as water does not contain significantly big particles, it does not cause scattering of light. Thus, at specified wavelengths water has no effect on light and can be left out from discussion. Scattering of dermis is predominantly caused by collagen, elastin fibers and their structures [55]. The most of light absorption in dermis occurs when interacting with the blood vessels and hemoglobin of blood [55, 58].

Table 3.3: Absorption and reduced scattering coefficients of human skin dermis. Data gathered from [55].

Wavelength, nm	Absorption,μa (mm$^-$1)	Scattering,μs (mm$^-$1)
600	0.2	3.2
700	0.16	2.6
800	0.13	2.2
900	0.08	2

As hemoglobin is the main absorber in dermis, it is expected that the blood should have similar absorption properties as dermis. However, as there are two types of hemoglobin (oxyhemoglobin and deoxyhemoglobin), their properties were considered separately (presented in table 3.4).

Table 3.4: Absorbance and reduced scattering coefficients for oxygenated (Hb $SatO_2$ 100%) and deoxygenated (Hb $SatO_2$ 0%) blood. Reduced scattering was calculated with equation 3.1, considering g=0.99. Data gathered from [58, 59].

	Absorption,μa (mm$^-$1)		Scattering,μs (mm$^-$1)	
Wavelength, nm	$HbSatO_2$ 100%	$HbSatO_2$ 0%	$HbSatO_2$ 100%	$HbSatO_2$ 0%
600	0.5	0.7	2.3	2.3
700	0.08	0.2	2.2	2.2
800	0.12	0.12	2	2
900	0.15	0.2	2	2

As can be clearly seen from table 3.4, oxygenation affects absorption ability of the blood. However, the variation is small because 800 nm is an isosbestic point of oxygenated and deoxygenated hemoglobin. Scattering of the light in blood is induced by high refracting index of hemoglobin (approximately 1.4), and stays nearly similar in the considered wavelength range [54, 58].

The next component of human tissue to be considered is subcutaneous fat, which is usually present under dermis. Similar to dermis, scattering of fat tissue is defined by thick collagen and elastin fibers. Due to presence of the blood vessels in subcutaneous fat, hemoglobin acts as absorber. Optical coefficients are summarized in table 3.5 [55].

Table 3.5: Absorption and reduced scattering coefficients of subcutaneous fat under human dermis. Data gathered from [55].

Wavelength, nm	Absorption,μa (mm$^-$1)	Scattering,μs (mm$^-$1)
600	0.2	2.5
700	0.15	2.2
800	0.1	2
900	0.1	1.9

According to table 3.5, fat absorbs in a similar way as epidermis and dermis at the considered wavelength range 600 nm to 900 nm, while the scattering is slightly below that of other tissue components. Consequently, subcutaneous fat does not have a dramatic effect on the light behaviour in comparison with skin.

Finally, the optical properties of the blood vessels walls are studied. The primary scattering source is the elastin fibers, and absorption occurs mostly

by blood due to presence of capillaries in the muscles. Jacques reports absorption coefficients as presented in table 3.6, and scattering coefficients are expected to be similar to dermis because elastin fibers dominate in the walls composition [60]. As table 3.6 demonstrates, the absorbance by the vessels walls is lower than by skin, meaning that passing through them will not cause significant attenuation of the light.

Table 3.6: Absorption and reduced scattering coefficients of the blood vessels walls. Data gathered from [55, 60].

Wavelength, nm	Absorption,μa (mm$^-$1)	Scattering,μs (mm$^-$1)
600	0.1	3.2
700	0.09	2.6
800	0.1	2.2
900	0.1	2

The comparison between reduced scattering coefficients of the skin parts, the blood vessels walls and the blood clearly shows that they have comparable scattering properties. Consequently, the movement of RBCs, which produces the frequency shift, is decisive in the laser Doppler phenomenon because scattering intensity from every tissue component is similar. When light penetrates the examined part of human body, it passes skin layers, fat and the vessels walls with some degree of absorbance and higher scattering. When it reaches the blood vessels, movement of RBCs insures that the scattered photons have the frequency shift, which can be detected and further analyzed. High anisotropy factor of both tissue and blood results in anisotropic forward scattering of photons, and consequently long path lengths before they leave the tissue and can be finally detected.

3.3 Therapeutic window

Therapeutic window (also known as optical window or near-infrared window), defines the wavelength range in which penetration of the tissue occurs with minimal light attenuation. Light attenuation is promoted by absorption. Therefore, the wavelength range, in which absorption coefficients for all tissue components are relatively low, is determined as therapeutic window.

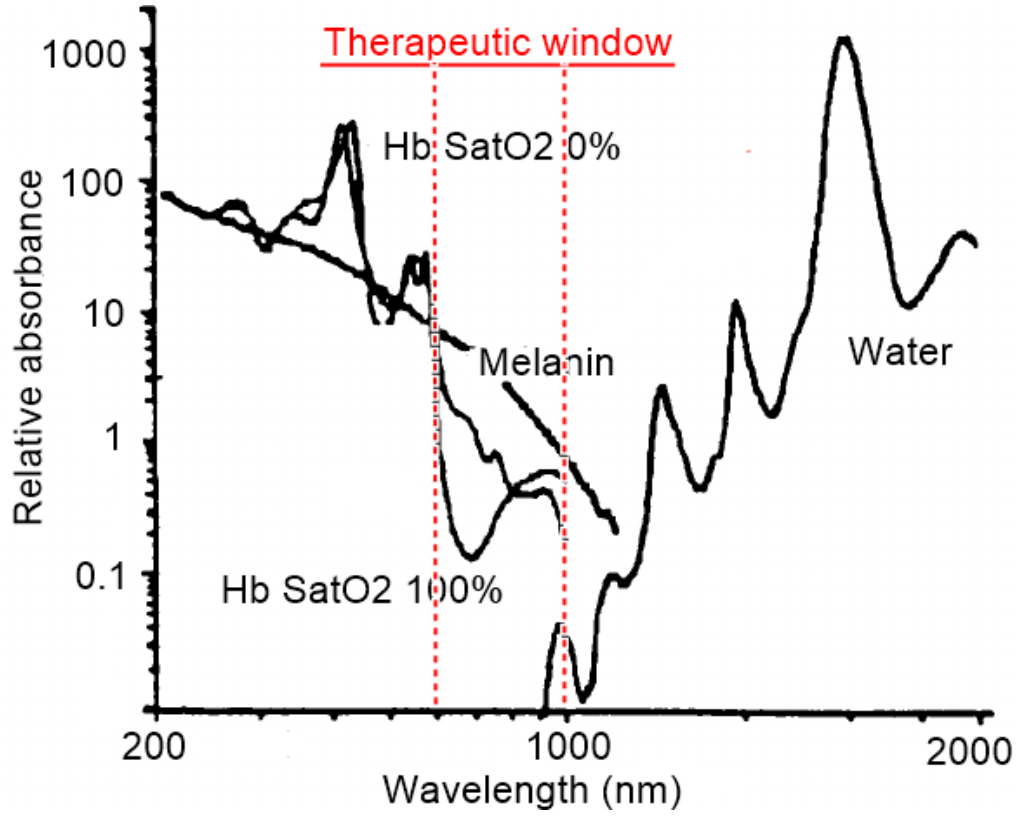

Figure 3.2: Therapeutic window is defined according to the relative absorbance of tissue components such as water, melanin, oxygenated and deoxygenated hemoglobin. Red lines determine the conventional window. Absorbance of oxygenated and deoxygenated hemoglobin and melanin at wavelengths over 1000 nm, and absorbance of the blood vessel wall are not indicated in presented figure. Adopted from [61].

Traditionally, therapeutic window is defined in the wavelength range of 600 nm to 1300 nm as shown in figure 3.2 [61, 62]. However, in order to minimize the gap between absorption of tissue components, the window in this work was reduced to 800 nm to 1000 nm range. One noticeable specific wavelength point is 800 nm because it is isosbestic point of hemoglobin at which Hb $SatO_2$ 0% and Hb $SatO_2$ 100% absorb equally. Consequently, the wavelength of around 800 nm can be an appropriate selection to minimize absorption by hemoglobin. Nevertheless, clear determination of suitable therapeutic window in particular measurement case assists in laser wavelength selection. Incorrect wavelength of the light leads to the light absorption before scattering, and, consequently, unreliable measurements.

Chapter 4

Design and experimental implementation

The practical implementation of this work comprised three parts based on theoretical considerations discussed in chapters 2 and 3. In chapter 4, laser and detector setups as well as optical phantoms and experimental procedures are described. Custom measurement setup and signal analyzing software were designed as demonstrated in section 4.1. Further, measurement procedures are discussed in section 4.2. Finally, functioning LDF setup is presented in section 4.3.

4.1 Design of the laser Doppler flowmetry measurement setup

The design of LDF measurement setup involved several steps. First, the laser system was planned according to the requirements declared by theory. Then, the measurement probes and the phantoms were designed in such a way that the experiments resemble real clinical needle procedures. Finally, data acquisition, recording and post-processing were carefully planned in order to obtain hight quality data from the performed measurements.

4.1.1 Laser system and measurement probes

The fundamental component of LDF measurement setup is the laser. The LD of 808 nm wavelength was used as a light source in this work. The decision to use such wavelength was made based on the considerations regarding the optical properties of human tissue and corresponding therapeutical optical

window described in sections 3.2 and 3.3. This wavelength is slightly attenuated by all tissue components, which provides a good base for meaningful experimental results. The power of the LD is another parameter, which must be carefully considered. Commercial LDF devices utilize very low power of 1 mW as was described in section 2.6. These instruments suit only microcirculation measurements, which are out of the scope of this work. On the basis of previous studies, which used the laser power of 50 mW, 70 mW and 120 mW [36, 44], it was assumed that the higher power should be considered for LDF setup. Besides, the laser optics introduces a certain level of power losses and the incident power of the laser beam is always lower than the actual LD power. Consequently, the LD of 100 mW power was implemented.

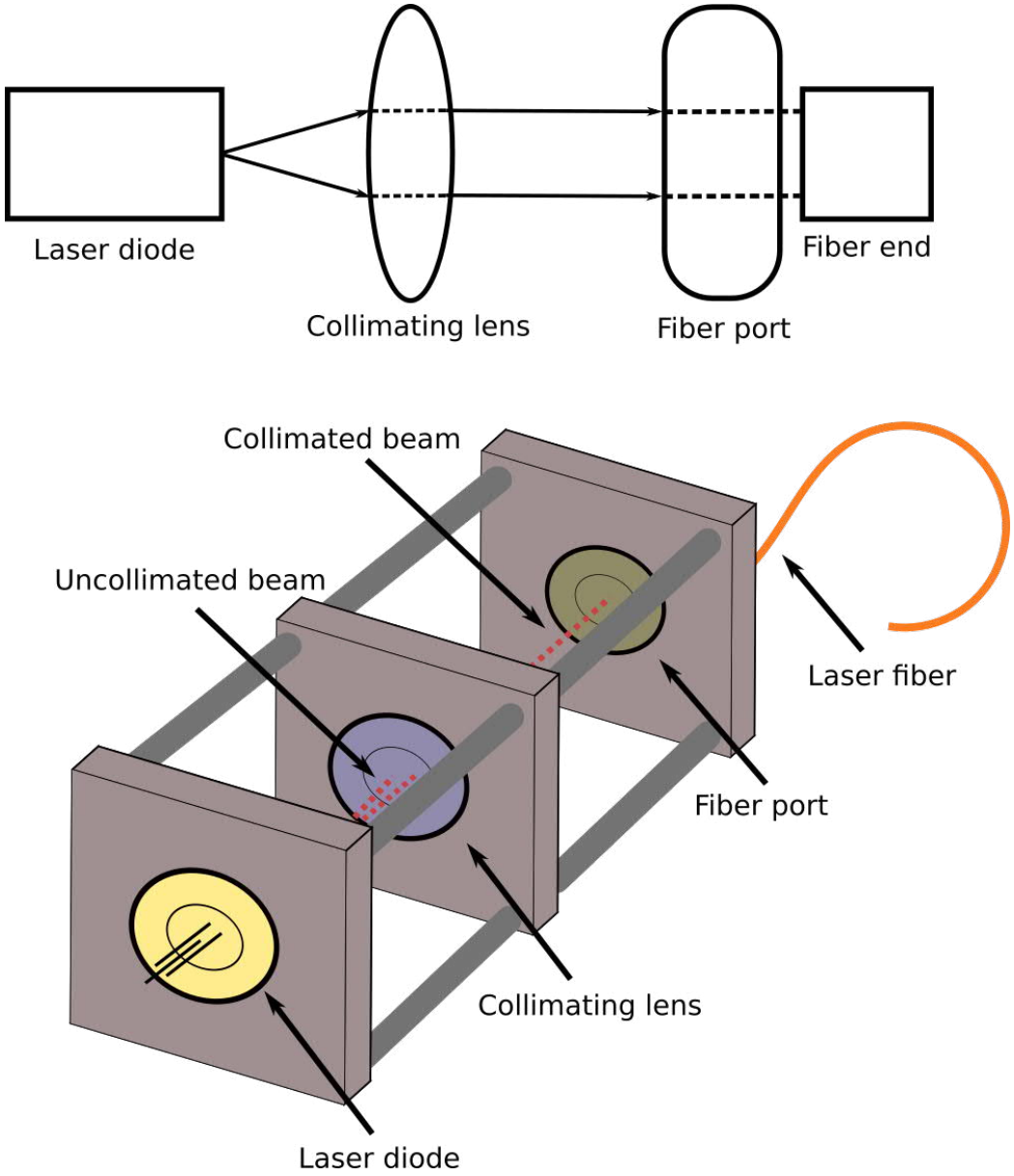

Figure 4.1: Schematic diagram and illustration of the laser-fiber collimation setup. The laser beam from the LD (not collimated) enters the lens, which collimates the beam to a certain diameter. Then the beam is directed into the fiber using the fiber port. The upper figure shows collimation mechanism. The bottom figure depicts the final design of the laser system.

As mentioned in section 4.1, two optical fibers are normally used, one as a source of the laser light and the other as a receiver of the backscattered light.

In order to connect the LD and the fiber, a certain collimation setup must be assembled as depicted in figure 4.1. First, the laser beam is collimated to a desired beam diameter using the lens with suitable focal length defined by the laser divergence angle. Then, special fiber port is used to direct the beam into the fiber. Single mode optical fibers require precise collimation, which is hard to achieve due to limited properties of the commercial optics. Thus, multimode fibers can be employed because they can receive the laser beam even if it is imperfectly collimated. However, it is important to understand that imperfect collimation, misalignment of the optics and multimode fibers introduce power losses, and the actual power of the laser beam from the fiber would be lower than the LD outputs. To reduce such laser attenuation, the system should be assembled with the alignment plates, as in figure 4.1, and collimation optics should be selected carefully.

Photodetector is another important part of the system. Silicon (Si) PD must be chosen because it can detect in 190 nm to 1100 nm wavelength range, which is in line with LD wavelength. Moreover, bigger active area of the PD provides better measurement accuracy because more backscattered photons are collected. Straightforward fiber coupling is an advantage of the PD because it eliminates the possibility of signal losses. Furthermore, the PD should have an embedded signal amplifier because the signal might be weak, especially at big fiber separation. It was decided to select commercially available PD, which suits the described requirements.

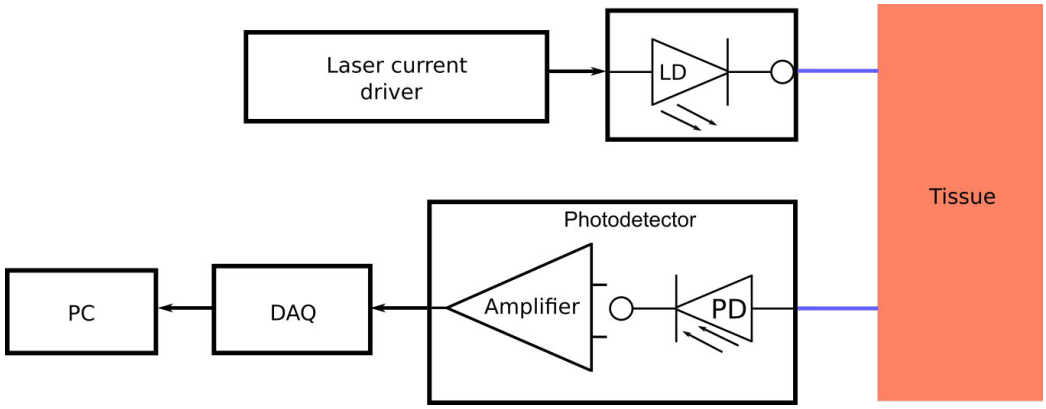

Figure 4.2: Schematic diagram of the experimental setup. Hardware consists of laser current driver, laser diode, photodetector, data acquisition device and PC.

The figure 4.2 depicts the principal schematic of LDF measurement setup. The laser current driver is selected based on the current requirements of the

LD. The signal from the photodetector is gathered with the data acquisition (DAQ) device through the high-impedance BNC cable and forwarded to the PC.

The design of the measurement probes is depicted in figure 4.3. The main requirements for the probes design are easy integration into the medical needle and different fiber separation distances. Two fibers can be inserted into the needle or alternatively the thin tube to provide the desired separation and good fixation inside. One fiber would supply the light from the laser diode and another would transmit the backscattered signal to the photodetector. The probe must be suitable for insertion experiments with the tissue-mimicking phantoms, as well as for superficial measurements with the mechanical phantom.

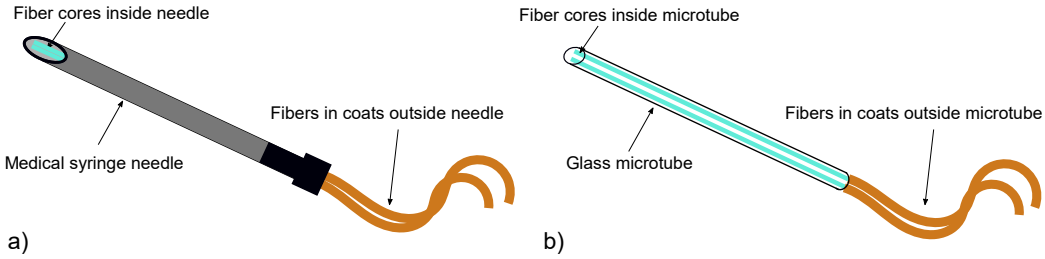

Figure 4.3: Schematic illustration of the probes for LDF experiments. (a) Needle probe: two 200 µm core diameter fibers are inserted into the medical needle forming 0.2 mm fibers separation. (b) Microtube probe: two 200 µm core diameter fibers are inserted into the glass microtube forming 0.7 mm fibers separation. The fibers are connected to the laser diode and the photodetector.

4.1.2 Design of experimental phantoms

Laser Doppler flowmetry setup must be evaluated in vitro using the phantoms before the tests with real human tissue can be performed. Not only the phantoms should resemble the optical properties of the tissue, but also they must have similar mechanical properties in order to reconstruct the needle procedures accurately. Two types of optical phantoms were planned in this work in order to evaluate the operation of the designed system. For that, the optical properties of the tissue and the blood were carefully compared with the properties of simulating materials. In particular, absorption and reduced scattering coefficients at 800 nm wavelength were correlated.

To simplify the modelling, the optical properties of epidermis, dermis, fat and blood vessel wall were considered as similar. According to tables 3.2,

3.3, 3.5, 3.6, the absorption coefficient at 808 nm wavelength is 0.13 mm^{-1} to 0.2 mm^{-1}, while reduced scattering is 2.2 mm^{-1} to 2.5 mm^{-1}. Blood has μa = 0.1 mm^{-1} and μs = 2 mm^{-1} at 808 nm as table 3.4 demonstrates. It means that the tissue and the blood can be actually presented by the same component, which has the following optical coefficients: μa from 0.1 mm^{-1} to 0.2 mm^{-1}, μs from 2 mm^{-1} to 2.5 mm^{-1}. It was found that 1.5% fat milk has similar optical properties as shown in table 4.1.

Table 4.1: The optical properties of 1.5% fat milk at 808 nm wavelength. Data gathered from [63].

Absorption,μa ($mm^{-}1$)	Scattering,$\mu s'$ ($mm^{-}1$)	Anisotropy factor,g
0.08	2.2	0.63

Anisotropy factor of milk is lower than of the blood. However, it is still relatively high, which leads to a certain degree of forward scattering of the photons. Absorption and reduced scattering coefficients are in line with coefficients of the real tissue components. Furthermore, the size of milk particles varies in the range of 1 µm to 10 µm [64], which correlates with the size of RBCs. Hence, the tissue model can be formed using milk, acting as scatterer and absorber. In order to make a substance, which has the mechanical properties similar to the tissue, gelatin can be added to milk [65]. Red ink mixed with gelatin models the color of the tissue. The blood can be simulated by aqueous solution of milk and water. Two phantom setups were constructed for the evaluation of different system capabilities.

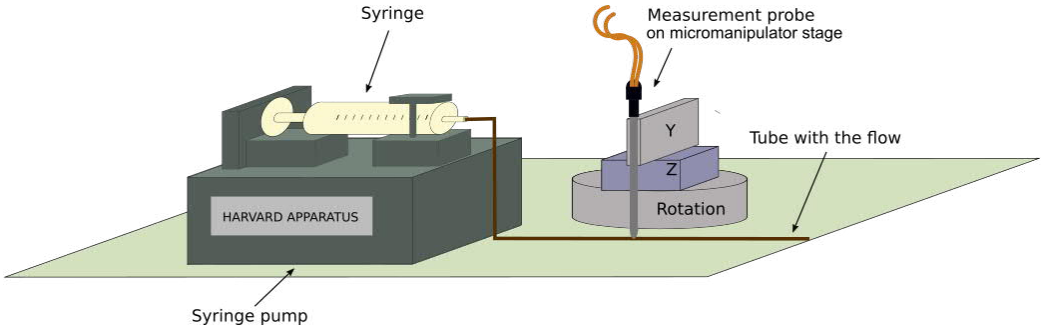

Figure 4.4: Schematic representation of the vessel phantom. A syringe is fixed in a syringe pump and supplies the flow to the tube. The measurement probe is mounted on the micromanipulator stage and touches the tube. Aspect ratio is not respected for better visualization.

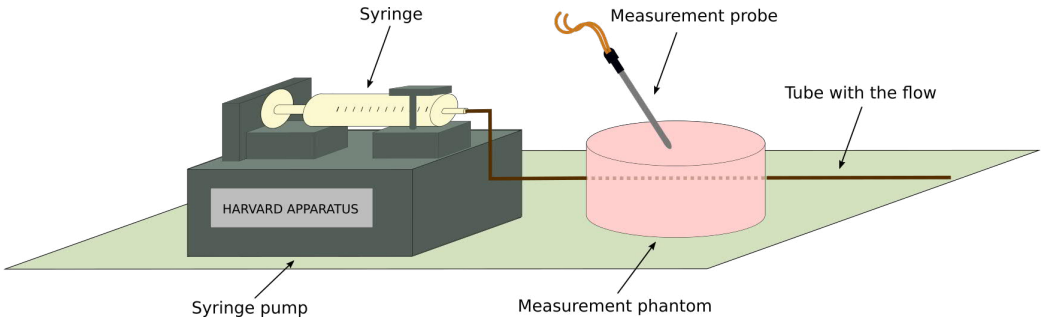

Figure 4.5: Schematic representation of the tissue phantom. A syringe is fixed in a syringe pump and supplies the flow to the tube. The tube is inserted into tissue-mimicking substance and models the blood vessel. The measurement probe is used to find the tube inside the simulated tissue. Aspect ratio is not respected for better visualization.

Figures 4.4 and 4.5 depict two phantoms designed according to the theoretical considerations discussed above. Both models utilize a pump to discharge the blood-mimicking liquid from the syringe into the tube to model the blood flow. It is important to select a tube, which does not reflect the light too much because extensive reflection of the photons can introduce errors to the measurement. The reflection level can be assessed by measuring the signal from the empty tube, and analyzing the detector output. It is desired that the detected signal does not rise in magnitude when the laser penetrates through the tube in comparison to the signal when the laser points to the air without obstacles in front of it. The principal difference between the phantoms is the measurement environment. The vessel phantom measurements are performed in the air (as presented in figure 4.4), while the tissue phantom (shown in figure 4.5) reproduces the real tissue environment. In such a way, all system capabilities can be evaluated employing the constructed phantoms.

4.1.3 Data acquisition software and signal analysis

Effective signal acquisition and analysis include real-time data output, as well as the possibility to record and post process the data. Consequently, two types of analysis algorithms were developed in this work. The first one was a program in Labview environment to output the actual data and record it when necessary. The second algorithm was used for the data post-processing in Matlab environment.

Figure 4.6 shows the block diagram of Labview software. It provides free

selection of sampling rate according to the requirements of the experiment defined by estimated size of the Doppler shift. In addition, AC and DC filtering can be controlled in a way that cutoff frequencies are easily varied, and order and type of the filter are freely changed. Furthermore, data recording can be arranged so that if enabled, a new file with unique name is created in designated folder and the data is stored with the sampling rate of acquisition.

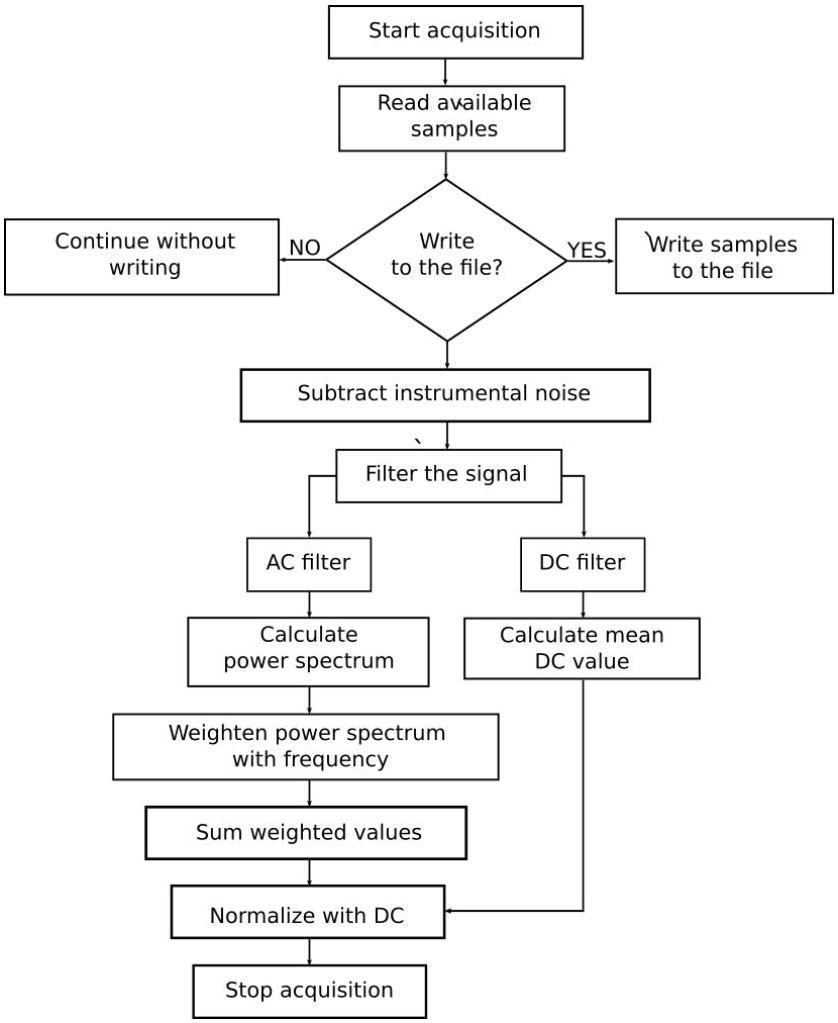

Figure 4.6: Block diagram of Labview software for data processing and representation.

Figure 4.7 depicts the block diagram of Matlab code flow, which was used for the data post-processing. First, the data collected with Labview software is imported into Matlab. It is filtered with the similar cutoff frequencies and

filtering parameters as in Labview software. Then it is divided into segments of a certain number of samples for better resolution of calculated perfusion. Next, Fourier transform with FFT method is calculated for the whole data in order to build the power spectrum, while FFT of segmented data allows perfusion calculation by weighting the power spectrum with the frequency. Processed data is represented in form of graphs for easy comparison of perfusion variations between the measurements.

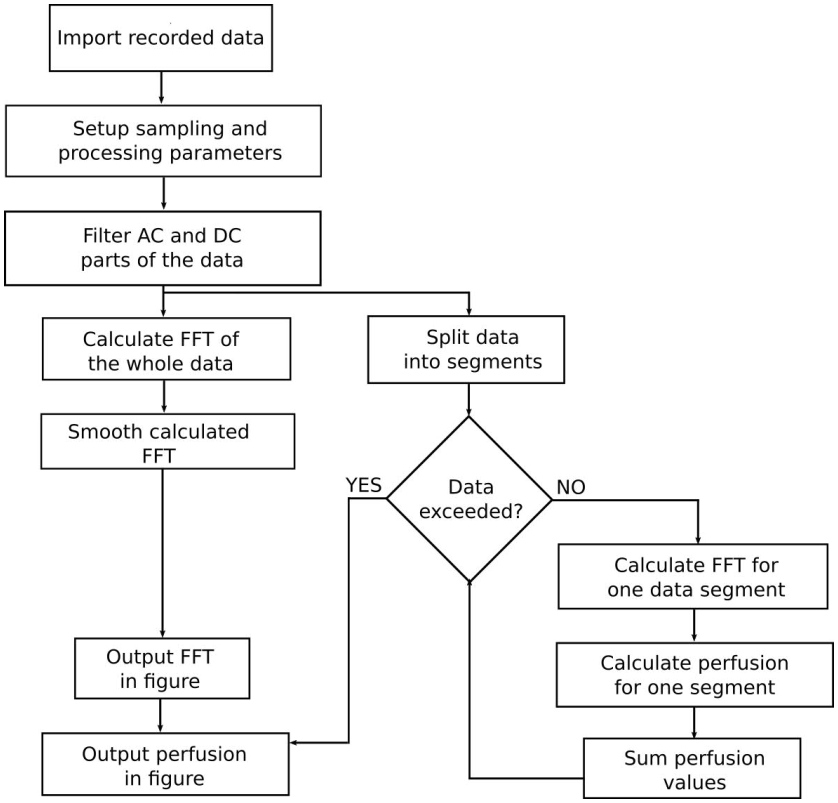

Figure 4.7: Block diagram of the Matlab code for data analysis.

4.2 Design of the measurement procedures

This section describes the experimental procedures that were designed for the assessment of LDF system capabilities. The first step before measurements was preparation of the system. Then, certain parameters of the flow

were assessed followed by experiments with the tissue-mimicking phantom. Finally, measurement range of the system was evaluated.

4.2.1 Calibration of the measurement setup

The calibration of the system is an essential step to obtain the noise parameters and evaluate the fibers separation effect. For the proper calibration, the noise parameters are calculated according to the discussion in section 2.3. The measurement probe must be attached to a piece of opaque plastic at different angles to measure DC voltage variations of the photodetector. Next, the perfusion value is measured and analyzed at each position. Finally, the first polynomial is calculated to obtain a linear function with two noise coefficients. Noise coefficients are utilized in software for noise subtraction during the real measurements.

The second step of system calibration is the assessment of the fibers separation effect. For that, two measurements probes, which were designed with different distances between the emitting and receiving fibers, can be used. The probes must be identically fixed as in the vessel phantom design with the same flow velocity inside the tube. Perfusion record with further post-processing must be performed in order to compare the signals and define separation effect.

4.2.2 Assessment of the flow parameters

The flow parameters must be assessed with both phantoms designed in this work. First of all, evaluation of the flow distinguishing capability shall be performed. For that, the vessel phantom can be used with varying flow velocity. Data must be recorded and post processed in Matlab providing comparison of the power spectra corresponding to each velocity. In principal, this procedure can reveal the possibility to separate different flows and speeds.

The next step is evaluation of the quality of perfusion measurements. It is expected from theory that the saturation of perfusion measurement would occur at certain velocity. When the saturation is reached, relative differentiation of flow velocities becomes impossible. Consequently, the measured perfusion can be plotted against the corresponding flow speed in order to visualize the saturation information. The CMBC measurement should be evaluated in a similar manner since the theory states that CMBC is identical at all velocities if the measurement volume and the number of moving particles in the flow are constant. In principal, the CMBC values plotted against

the matching flow speeds should follow the linear regression with the slope equals 0.

To confirm that similar measurements can be performed in non-air environment, the flow parameters evaluated with the vessel phantom must be assessed with the tissue phantom. As the design of the tissue phantom is based on the optical properties, it is expected that experiments would provide similar results as if LDF measurements were performed in real tissue. First, the possibility of blood vessel detection must be demonstrated. The tube inside the tissue phantom shall be located with the measurement probe. The data can be observed in real-time and recorded for further post-processing. Successful blood vessel detection would result in increased perfusion value in comparison to the base signal inside the phantom. The second step is evaluation of the flow speeds differentiation. The probe must be fixed on the tube inside the phantom with the flow velocity varied in the detectable range (below saturation velocity). The increase in perfusion measurement is expected to follow the trend of the vessel phantom experiments results.

4.2.3 Evaluation of the measurement range

The last part of the system evaluation is determination of the measurement range. Several parameters must be defined in order to evaluate the capabilities of the designed setup: penetration site, penetration depth and penetration angle. All parameters can be estimated utilizing the vessel phantom design.

The penetration site defines the location of the laser beam during the measurement. The blood vessels have various diameters, however, big vessels such as arteries and veins are in the interest of this work. Consequently, penetration through the wall of the vessel is possible in real measurements because its diameter can be bigger than that of the laser beam. Figure 4.8 depicts the penetration points that must be assessed. One point is the penetration right through the flow inside the tube. At two other points, partial penetration through the wall of the tube with different portions of the light going through the flow shall be analyzed. The change in perfusion with the flow velocity must be checked in order to define at which position the measurement is still possible.

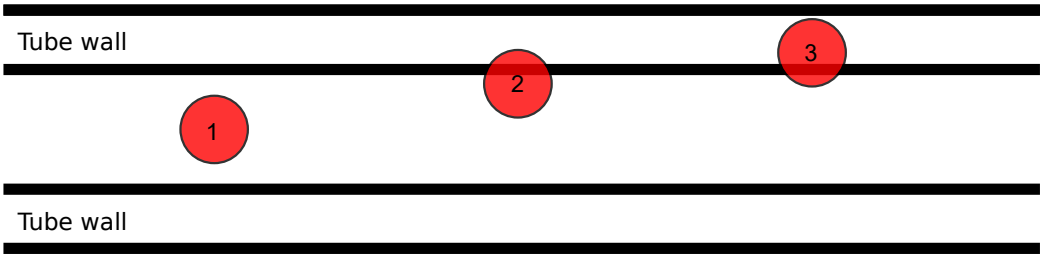

Figure 4.8: Experimental schematic of the penetration site assessment. Red circles indicate the laser penetration points. At point 1, the laser penetrates through the tube. At point 2, the biggest portion of the beam goes thought the tube and some portion penetrates through the wall of the tube. At point 3, almost whole beam goes through the wall with the minor portion penetrating the flow.

The penetration depth is extremely important in the needle procedures, which are the primary application in this work. Consequently, it is important to measure the maximum distance at which blood vessel detection is possible. Figure 4.9 depicts three measurement configurations. Direct contact between the probe and the tube is the starting position because all evaluation measurement are performed in this configuration (presented in figure 4.9 (a)). The next positions represent the increasing distance between the probe and the tube (shown figures 4.9 (b) and (c)). However, the measurement does not simulate the real situation if there is air in between. Consequently, a piece of the tissue-mimicking material from the tissue phantom can be used. The maximum tissue thickness, through which LDF measurement is possible, defines the penetration depth value of the system.

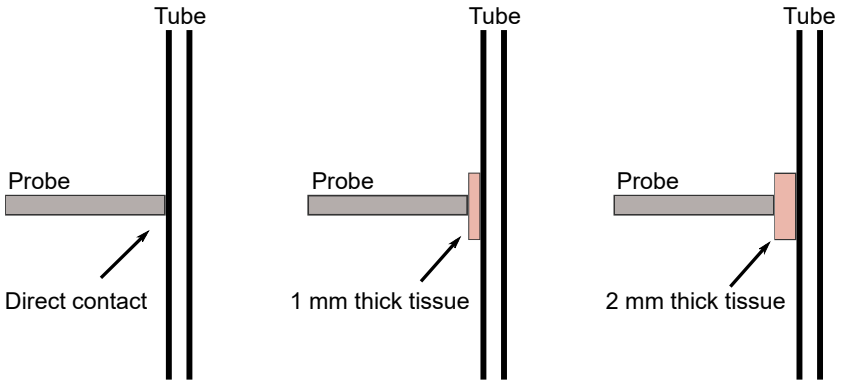

Figure 4.9: Experimental schematic of the penetration depth assessment. Positions other than the direct contact (a) employ a piece of tissue-mimicking material of certain thickness in between (b-c).

The last parameter of the system is the penetration angle. Usually, the needles are inserted at certain angle, which is hard to accurately predict due to anatomical variations of the blood vessel location. According to theory, the maximum Doppler shift is achieved when the laser beam is orthogonal to the flow, however, the varying angle should not lead to full degradation of the signal. Thus, LDF measurement should be possible at small angles between the needle and the blood vessel. Consequently, it is desired that measurement angle range is as big as possible, and it can be assessed as depicted in figure 4.10.

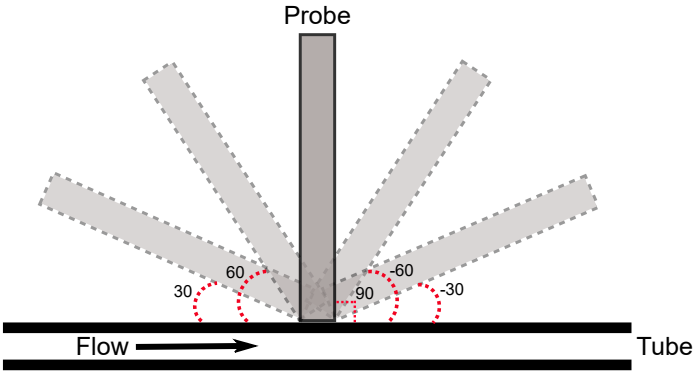

Figure 4.10: Experimental schematic of the penetration angle measurements. Probe position is varied with 30° steps to both sides starting from the position perpendicular to the tube.

The figure 4.10 demonstrates that the initial measurement angle is 90° meaning that the probe is perpendicular to the flow. Then the angle is varied in both directions with 30° step, and perfusion measurement quality must be assessed. Due to fibers core diameter, certain limitation of the measurement angle is expected because laser light penetrates mostly through the wall when the angle to the tube is low.

4.3 Experimental setup

Experimental setup was built based on the design and schematics presented in section 4.1. Figure 4.11 demonstrates the assembled measurement system.

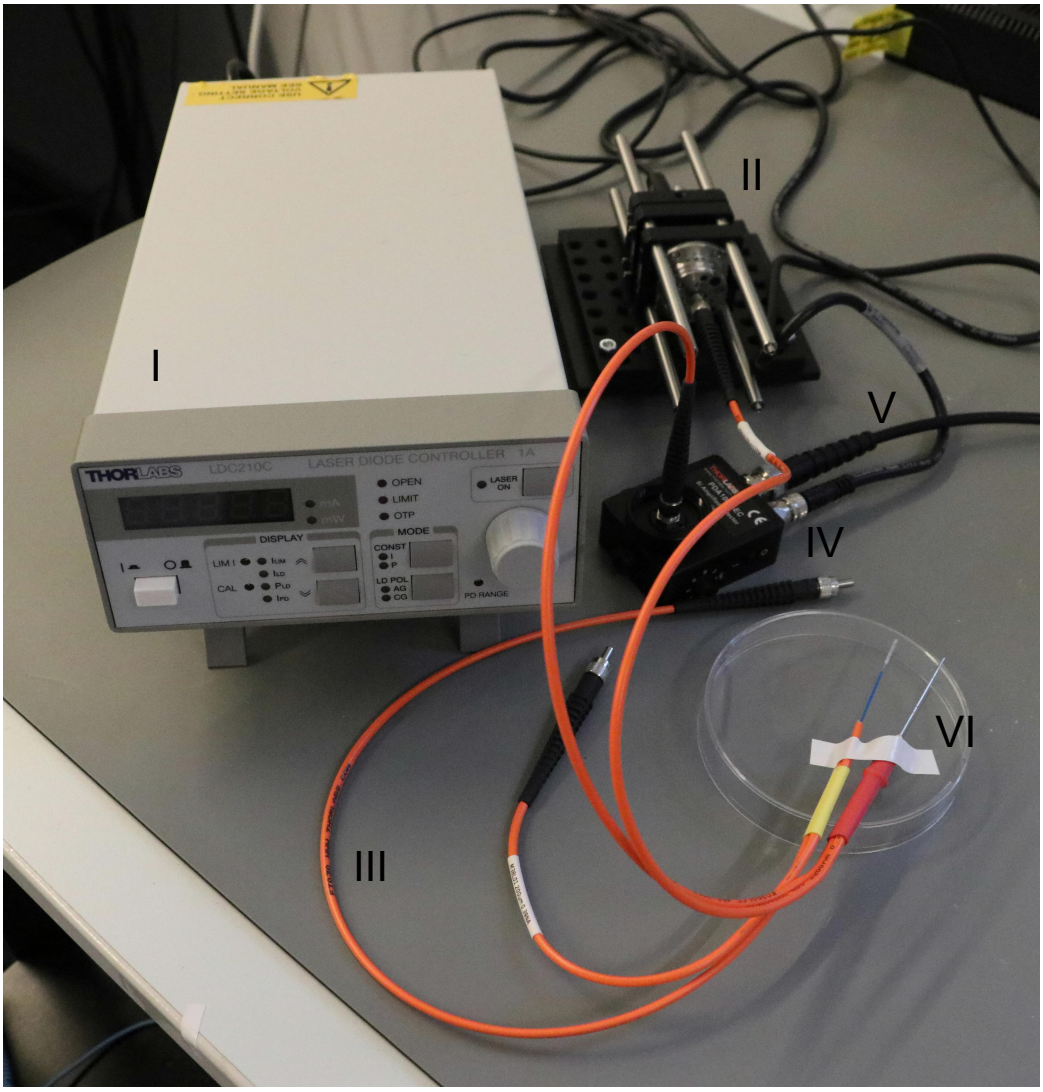

Figure 4.11: Measurement setup that contains laser current drive (I) and laser collimating system (II) with multimode fiber (III) on the output. Same multimode fiber is connected to the photodetector (IV), which outputs the signal to the data acquisition device via Bayonet Neill-Concelman (BNC) cable (V). Ends of the fibers are combined into two types of probes (VI). Data acquisition device is not visible in figure.

In the measurement setup, laser current driver (LDC210C, Thorlabs) supplied current to the preliminary collimated LD (LD808-SA100, Thorlabs). Collimation of the LD was implemented with aspheric lens with 3.1 mm focal length (C330TMD-B, Thorlabs), and the laser beam was directed into the

fiber with the fiber port (PAF-SMA-5-B, Thorlabs). The laser system was assembled utilizing 30 mm cage plates (CP02/M, S1LDM9 and CP1TM09/M, Thorlabs) with suitable adapters for the LD, the lens and the fiber port. The plates were fixed with assembly rods (ER6-P4, Thorlabs) that provided reliable fixation of the components. Backscattered signal was collected by Si photodetector with embedded amplifier (PDA100A, Thorlabs). The detector had big active area (100 mm^2) which insured that the most of backscattered photons were collected. NI USB-6363 (National Instruments) data acquisition device (not visible in figure 4.1) acquired the signal from the detector and was further processed using PC in Labview or Matlab environments. The selected DAQ instrument had an analog input with BNC connector identical to the output of the detector, eliminating the necessity of cable conversion, which might introduce noise to the measurements.

The first probe utilized two multimode fibers with core diameter of 200 µm and numerical aperture (NA) of 0.39 (M38L01, Thorlabs), which were inserted into the medical injection 22G needle resulting in 0.2 mm fiber separation. The needle of 22G was selected for evaluation experiments because its inner diameter is 0.41 mm meaning that the needle can accommodate two 200 µm fibers inside [66]. In such configuration, the fibers are tightly fixed and do not move, which is an advantage because movement of the fibers inside the probe introduces noise to the measurements as was already mentioned in the previous chapter. However, for real applications bigger needles can be utilized although it will require additional fiber-fixing mechanism.

The second probe was built with identical fibers in the same configuration as the first probe, but placed inside the glass microtube. Glue was used to fix the fibers inside the tube. In this configuration, the distance between the fibers was 0.7 mm, which is bigger than in the first probe. As the microtube probe is not suitable for insertion experiments, it was used in evaluation of the fiber separation effect. Cleaning of both probes was done with isopropyl alcohol and lens tissue.

The vessel phantom was a flow simulation with the static probe fixed in micromanipulator, as figure 4.4 demonstrates. The plastic tube with inner diameter of 0.5 mm or 1 mm, and the wall thickness of 0.5 mm or 0.75 mm, and manufactured from low reflecting material, acted as a blood vessel. Milk (1.5%, pasteurized, Valio) flowing in the tube was diluted in DI water in concentration 1:1 and simulated the blood flow. The milk solution was stirred in the magnetic stirrer for 10 minutes before each experiment to avoid agglomerated particles, which can cause measurement errors.

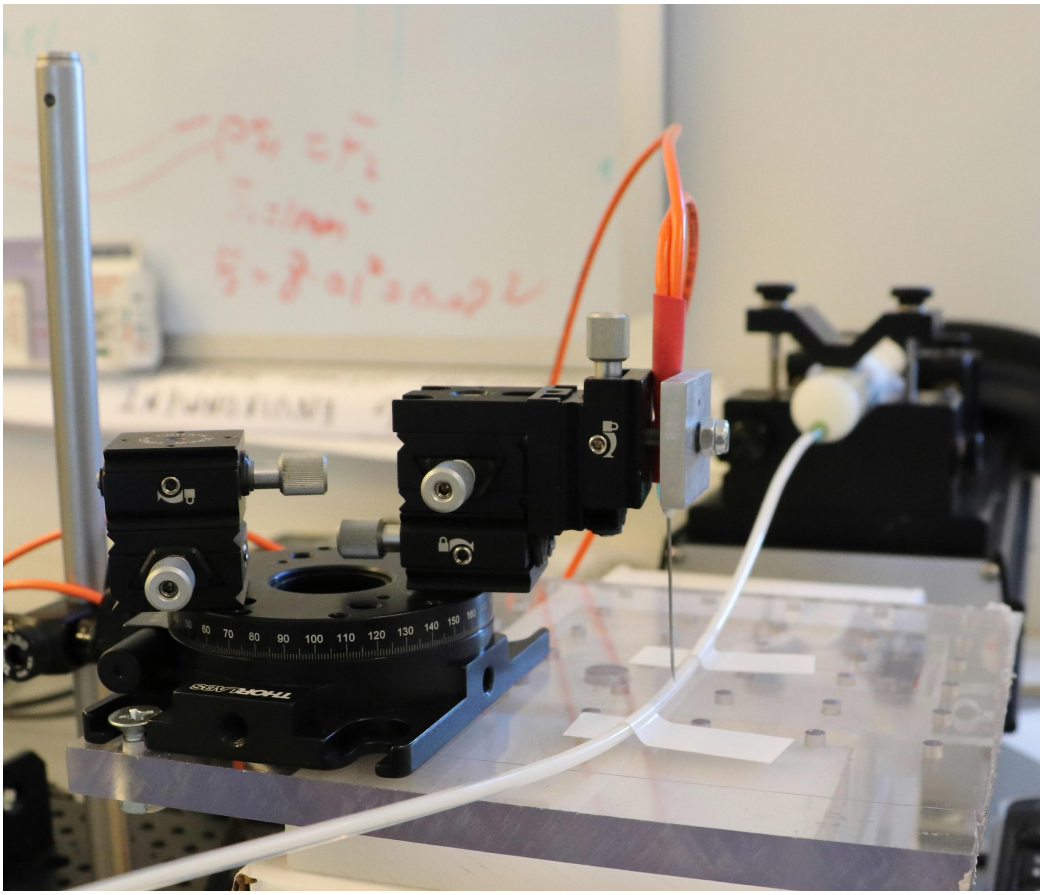

Figure 4.12: Photo of the vessel phantom. The real phantom replicates the schematic in figure 4.4 presented in the previous section 4.1.

A syringe pump (PHD ULTRA, Harvard Apparatus) discharged the liquid from the syringe to the tube, producing the flow with constant velocity. Disposable medical syringes of 20 ml volume (BD Medical) were used in all experiments. Better results were obtained with the new syringe because the syringe injects smoothly only a few times. Thus, it should be disposed after 2 or 3 cycles and replaced by the new syringe. The flow velocities from 0 mm/s to 10 mm/s with 1 mm/s step was tested. The evaluation of measurement range was performed utilizing the vessel phantom with variable positions of the probe (as was described in the previous section). The measurement data was monitored and recorded in real-time for further processing in Matlab as described in the following section.

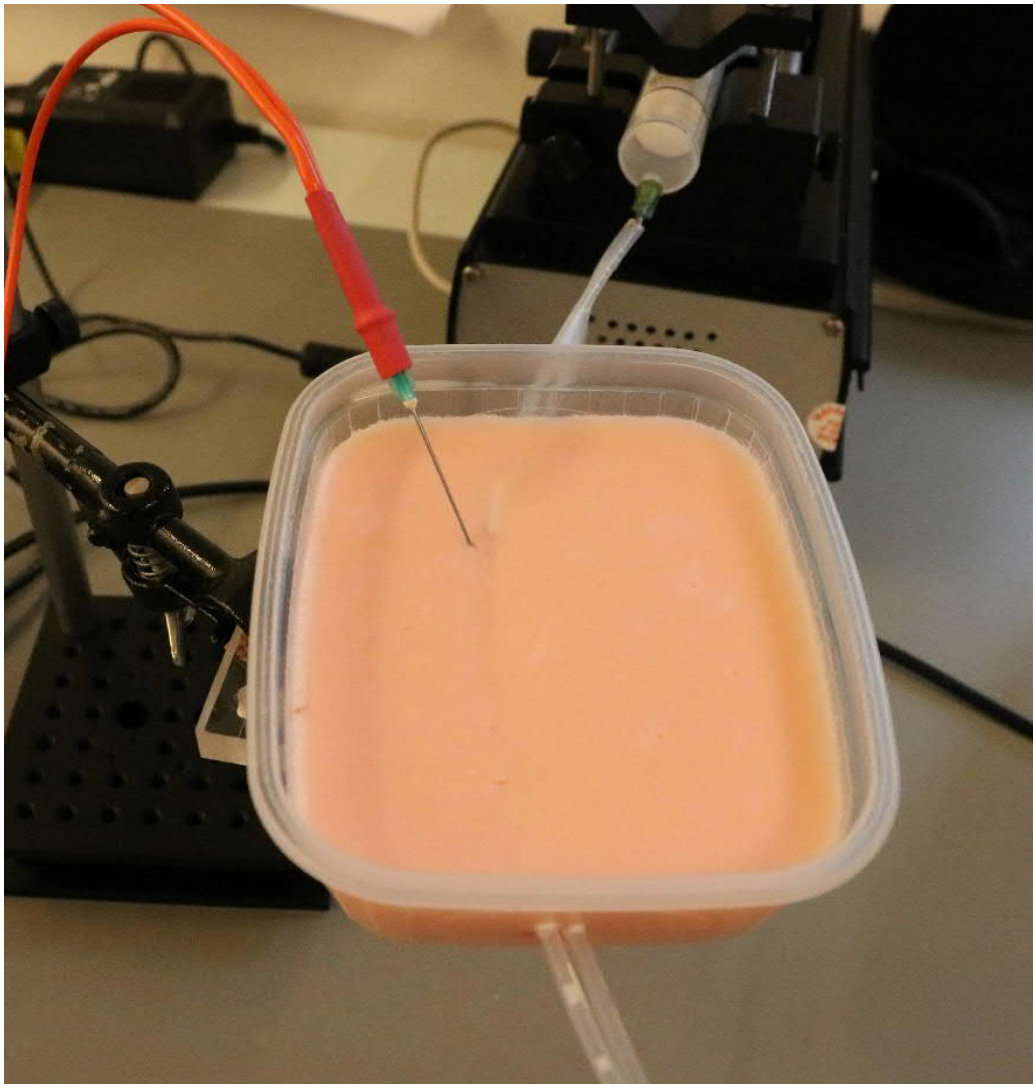

Figure 4.13: Photo of the tissue phantom. The real phantom replicates the schematic in figure 4.5 presented in the previous section 4.1.

The tissue phantom was a tissue-mimicking model presented in figure 4.13. Gelatin manufactured from bovine skin (Type B, 225 g Bloom, Sigma-Aldrich) was dissolved in solution of milk (1.5%, pasteurized, Valio) and DI water. The concentration of milk and water was 1:1, and gelatin comprised 15 g for 200 ml of liquid. The solution was stirred in the magnetic stirrer at 80° for 15 minutes until gelatin was fully dissolved. Red ink was added to achieve pink color of the substance. Transparent containers with plastic tubes going through them were filled with gelatin solution and kept in refrigerator

for 2 hours until firm gelling. For the blood flow simulation, milk was mixed with DI water in concentration 1:1. In the tissue phantom experiments, the measurement probe was manipulated manually by approaching the tube inside gelatin model. An identical range of flow velocities (from 0 mm/s to 10 mm/s with 1 mm/s step) as with the vessel phantom was tested. The measurements were monitored and recorded in real-time and post processed in Matlab.

The data processing was implemented in two different ways, which were described in the previous section 4.1. The real-time data representation and recording were realized with Labview software, while subsequent data analysis was completed in Matlab. Real-time mode was important and useful in the experiments with tissue-mimicking phantom because an immediate observation of the detector output was required. Data recording was especially useful in the static experiments with constant flow speed and fixed probe (the vessel phantom), because further data processing provided convenient comparison of the results from different measurements. The interface of real-time acquisition program is presented in figure 4.14.

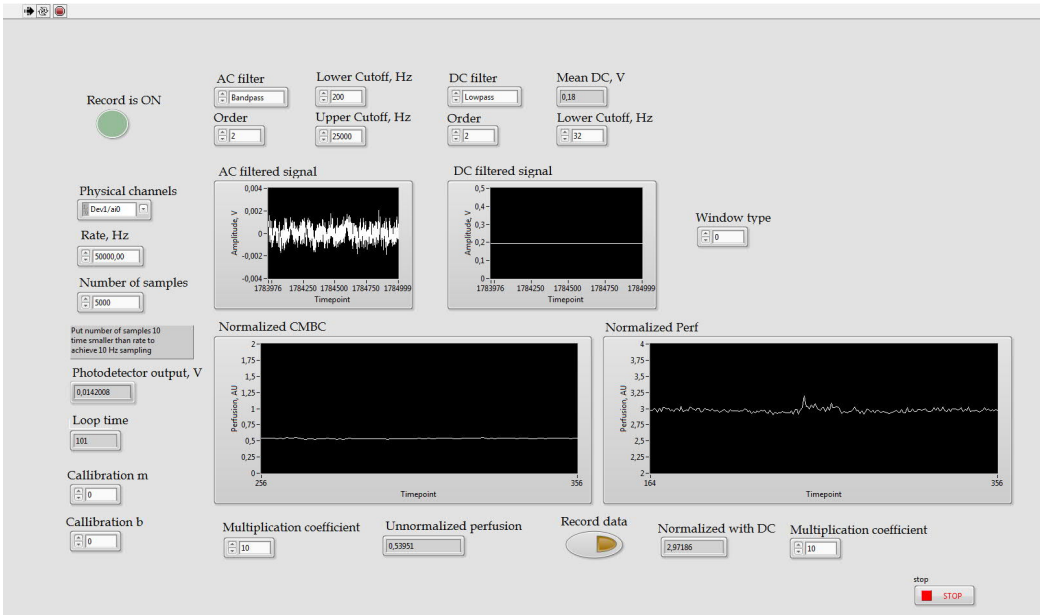

Figure 4.14: Labview program interface for real-time data representation. Chart "Normalized Perf" outputs calculated perfusion values; chart "Normalized CMBC" displays the concentration of the flow; charts "AC filtered signal" and "DC filtered signal" show AC and DC part of the signal correspondingly; "Record data" button creates new file with real-time data, starts and stops writing; all settings of the data acquisition are freely set.

Necessary sampling rate for the data acquisition with both Labview and Matlab was calculated according to equation 2.19. Low speeds in the range of 0 mm/s to 10 mm/s were used for the measurements, and the laser wavelength was 808 nm, providing that expected Doppler shift was at maximum 25 kHz. Consequently, according to Nyquist theorem, sampling rate of 50 kHz was used in the measurements. The cutoff frequencies of the AC filter were 200 Hz and 25 kHz, while DC limit was set to 32 Hz.

Chapter 5

Results and discussion

Chapter 5 provides results of the experiments implemented according to the design described in the previous chapter 4. First, calibration of the measurement setup and fiber separation effect are presented in section 5.1. Further, results of general evaluation of the system, including velocity differentiation capability, measured Perf and CMBC trends, are demonstrated in section 5.2. Then, further assessment of system potential and confirmation of operation in tissue-mimicking environment are depicted in sections 5.3 and 5.4. Finally, applicability of technology and possible improvements are discussed in section 5.5.

5.1 Calibration measurements and fiber separation effect

The first step of signal processing was calibration for evaluation of instrumental noise. The needle probe was attached to a piece of opaque plastic at six different angles in order to measure DC level of PD signal and calculate the corresponding perfusion. On the basis of these measurements, linear fitting was performed in order to estimate the noise coefficients. Figure 5.1 depicts the calibration result.

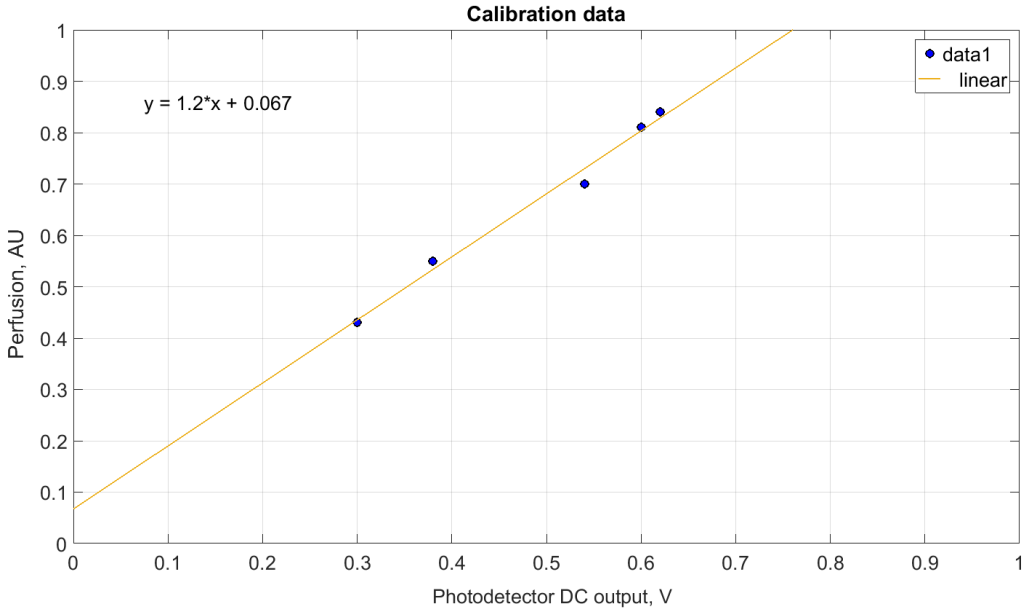

Figure 5.1: PD noise calibration measurements. X axis indicates DC level of PD signal, while Y axis expresses the corresponding perfusion. Yellow line represents linear fit of the data.

As shown in figure 5.1, the linear fit provided noise coefficients of $m = 1.2$ and $b = 0.067$. Later these coefficients were used during normal LDF measurements for actual noise calculation and further subtraction from perfusion measurements, as was demonstrated in equation 2.18.

The fiber separation effect on the measured signal was studied prior to the actual phantoms experiments. For this, two probes with different fibers separation (needle probe with 0.2 mm and microtube probe with 0.7 mm separation) were evaluated with vessel phantom setup. Constant flow was supplied through the tube, the data was recorded and post processed in Matlab. Figure 5.2 depicts calculated perfusion obtained with each probe.

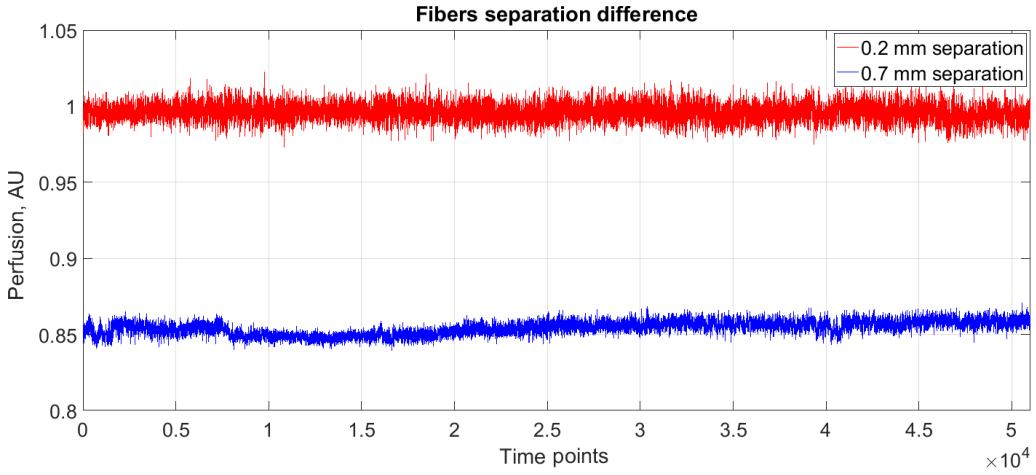

Figure 5.2: The perfusion measurements obtained by different probes with 0.2 mm (red) and 0.7 mm (blue) fiber separation. X axis indicates the time point of the measurement defined by the selected segment length, while Y axis expresses the calculated perfusion in AU.

Figure 5.2 clearly demonstrates that the intensity of the signal is smaller at bigger fiber separation, which is well in line with theory. Reflection from static structures dominates in LDF measurements, especially when the fibers separation is small. Increased separation leads to reduced signal from the static parts, however, the probability that the Doppler shifted photon is gathered by detector is higher. Consequently, a small fiber separation provides more intense signal, which contains photons scattered from RBCs near the surface of the skin, while bigger separation allows deeper penetration and scattering from more in-depth RBCs with reduced total light intensity. Nevertheless, the penetration depth cannot be infinitely increased by adjustment of the fiber separation value, as demonstrated in the following sections.

5.2 Evaluation of laser Doppler flowmetry capabilities

The main purpose of experiments with the vessel phantom was to assess if differentiation between different flow velocities is possible. It was expected that the power spectrum would become wider with increased velocity as was stated in section 2.3.3. Figure 5.3 depicts the result of the measurements that

were processed in Matlab. The data was acquired using Labview software with 50 kHz sampling rate. Velocities in the range from 0 mm/s to 10 mm/s were evaluated.

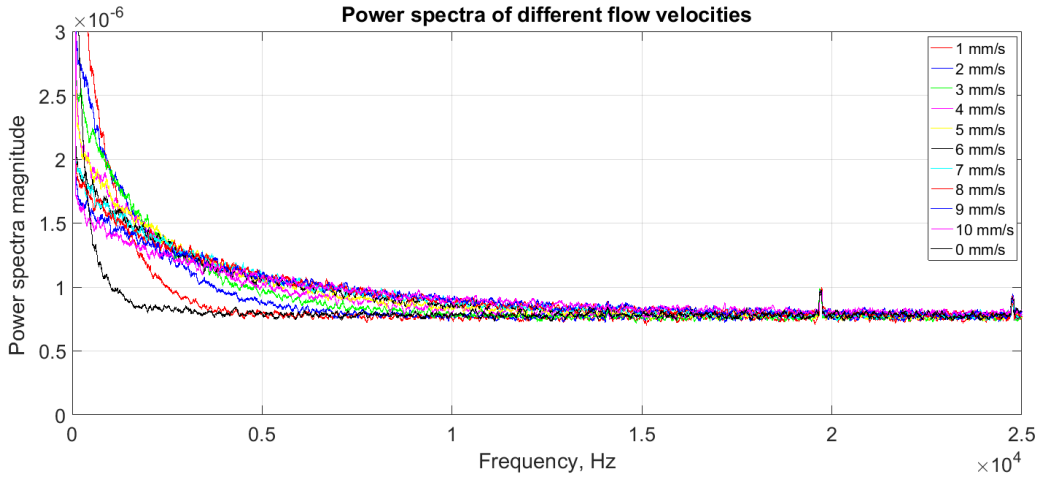

Figure 5.3: Power spectra of 11 different measurements, where each represents one velocity of the flow. Velocities of 0 mm/s to 10 mm/s with 1 mm/s step are evaluated. X axis indicates the frequency of the Doppler shift in Hz, while Y axis expresses the power density of the signal at each frequency.

From figure 5.3 it is clearly observable that power spectrum widens, which coincides with theory. When velocity of the flow increases, the Doppler shift value increments resulting in more frequencies included in the beating frequency as indicated in the power spectrum graph. In figure 5.3, power spectra demonstrate that 1 mm/s flow induces the Doppler shift below 500 Hz, while 10 mm/s flow generates a frequency shift up to 17 kHz. To confirm the trend, perfusion values of the same measurements, as were depicted in figure 5.3, were calculated and plotted against the flow speeds. The mean value of five trials with standard deviation is presented in figure 5.4.

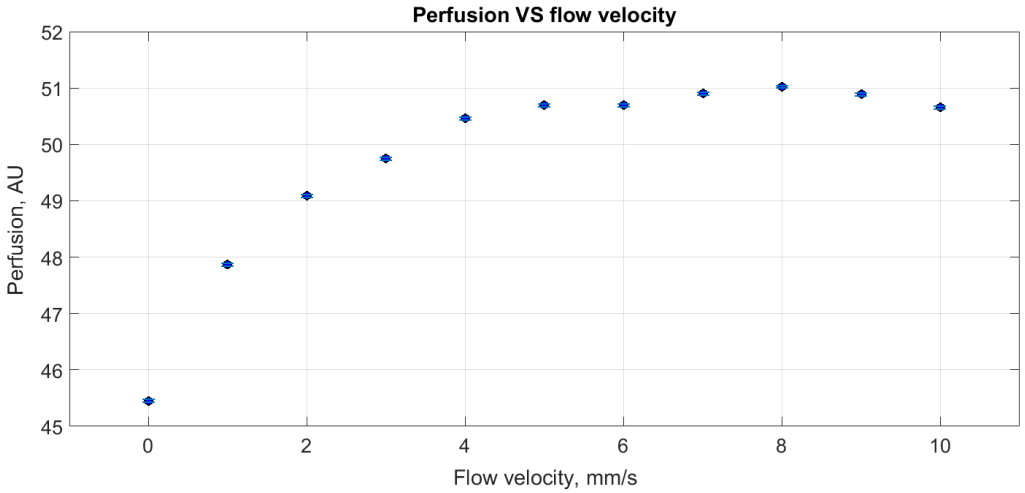

Figure 5.4: The perfusion trend increasing with the speed of the flow. X axis indicates the speed of the flow in mm/s which are known from the pump, while Y axis expresses the calculated perfusion in AU. The mean value of five trials with standard deviation is presented.

From figure 5.4, we can conclude that perfusion measurement saturates with increasing velocity of the flow. The reason for such trend is unclear but we suggest that at higher velocity multiple scattering of the laser light prevails leading to both positive Doppler shifts, which are cancelled out in the detector and only few single shifts are eventually detected. The consequence of perfusion saturation is an inability to recognize the high blood flow speeds, which prevail in big blood vessels such as aorta or venae cavae. However, identification of slow blood flows is still possible as well as the distinction between slow and fast blood flows. Such case can be encountered in human body when the needle probe is moving from the surface of the skin in the direction of the femoral artery. In this situation, the microcirculation in dermis with the flow velocity less than 1 mm/s can be easily distinguished from the blood flow in the artery, which has flow velocity of around 500 mm/s. However, the differentiation of such artery from the vein with flow velocity of 100 mm/s might be impossible with LDF system developed in this work. It has to be noted, that at low blood flow velocities, nearly linear trend of the perfusion was observed, which makes the technique suitable for the blood flow applications where flow velocity does not exceed 8 mm/s.

In the measurements discussed above, the position of the probe was kept the same at all velocities meaning that the fraction of moving particles in the examined volume was stable. As was explained in section 2.3.3, calculation

of CMBC allows to estimate the concentration of moving RBCs in the flow. Consequently, CMBC was evaluated by calculating zero moment of the power spectrum. Figure 5.5 demonstrates CMBC trend at different flow velocities. The mean value of five trials with standard deviation is presented.

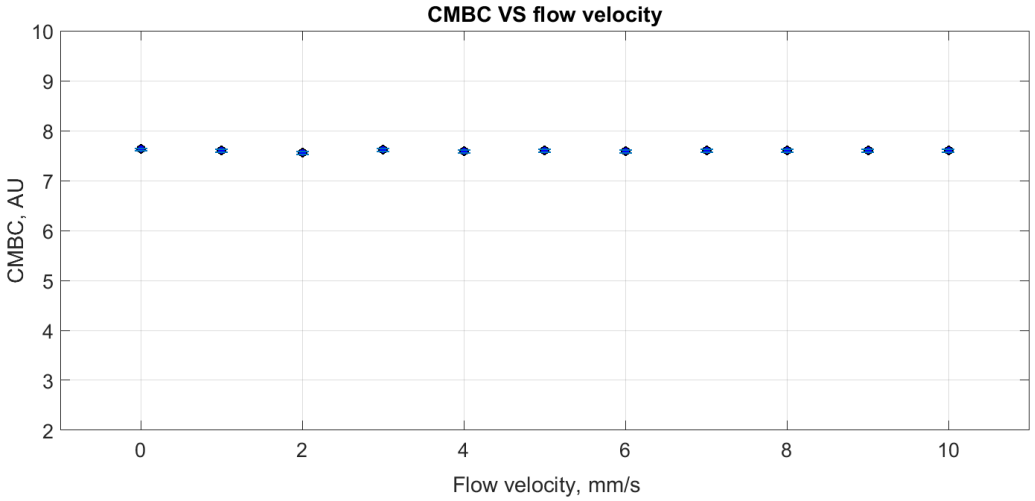

Figure 5.5: The CMBC trend that stays constant with increasing speed of the flow. X axis indicates the speed of the flow in mm/s which are known from the pump, while Y axis expresses the calculated CMBC in AU. The mean value of five trials with standard deviation is presented.

The final test needed for the initial evaluation of created LDF system was the assessment of varying concentration at constant flow speed. Four different milk fractions in DI water (25%, 50%, 75%, 100%) were considered. The speed was constant at each concentration. Figure 5.6 represents how varying concentration of the flow affects the perfusion measurement. The mean value of five trials with standard deviation is presented.

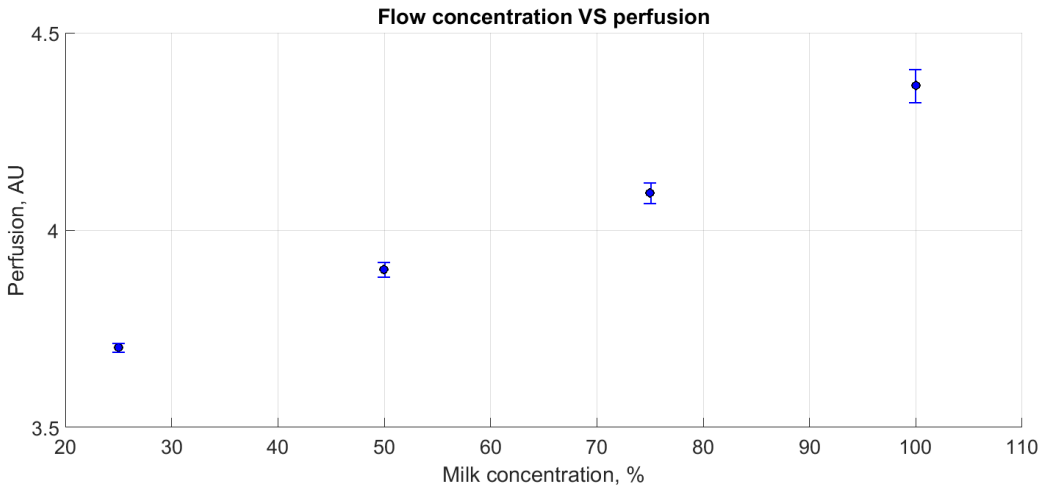

Figure 5.6: Trend of perfusions values increasing with the increased concentration of the flow. X axis indicates the concentration of the flow defined by the milk content, while Y axis expresses the calculated perfusion in AU. The mean value of five trials with standard deviation is presented.

According to figures 5.4 - 5.6, perfusion measurement undergoes definite saturation at high flow velocities, while CMBC measurement is evidently unaffected by velocity variations provided that constant concentration of the flow is presumed. Moreover, increasing fraction of the moving particles leads to increased perfusion, which is expected because more scattering objects are introduced. These trends perfectly correlate with the results presented by Leahy et al. [18] and Figueiras et al. [33]. On the basis of performed evaluation experiments, it was concluded that the functioning LDF system was successfully designed and implemented. The setup works similarly to commercially available and custom LDF monitors. The next step was to assess whether the system can be used in the blood vessel detection procedures.

5.3 Measurement ranges of the system

The measurement ranges of LDF system were assessed as described in section 4.2. The needle probe was used in all experiments except evaluation of the penetration depth when the microtube probe was also utilized. Five cycles of each experiment were run in order to obtain standard deviation of the data. First, the penetration site was evaluated. Figure 5.7 depicts the

variation of the perfusion measurements at three penetration sites referred to as measurement points.

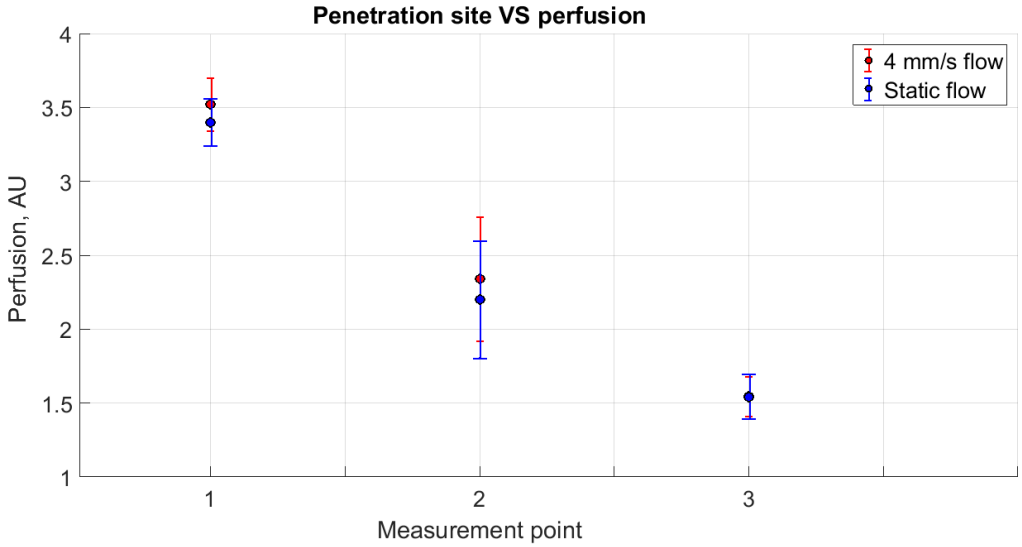

Figure 5.7: Dependence of the perfusion measurement on the laser penetration site. Blue and red markers denote the flow with 4 mm/s velocity and the static flow respectively. At point 1, the laser penetrates through the tube. At point 2, the biggest portion of the beam goes thought the tube and some portion penetrates through the wall of the tube. At point 3, almost whole beam goes through the wall with the minor portion penetrating the flow. X axis indicates the measurement point as was defined in section 4.2, while Y axis expresses the calculated perfusion in AU. The mean value of five trials with standard deviation are presented.

The strongest signal and the most significant perfusion increase with the flow velocity is observed when the laser beam penetrates through the center of the tube or the blood vessel. Partial penetration through the wall leads to certain degradation of the signal although determination of the flow is still possible. Finally, penetration primarily through the wall of the tube or the vessel results in even further signal attenuation, and the flow cannot be distinguished any more. Such tendency is evident because when the laser passes through the wall, less photons are scattered from the flow and less amount of meaningful signal is collected in the detector. From this result, it can be concluded that the blood vessel can be detected if the probe points exactly into it. Depending on the size of the vessel, some portion of the laser can penetrate through the wall without measurement errors.

The second assessment step was estimation of the penetration depth. Figures 5.8 - 5.9 show the results of experiments with different distances between the probe and the tube. Two probes with 0.2 mm and 0.7 mm fibers separation were evaluated. Similar to penetration site study, the flow with 4 mm/s and the static flow were compared in order to define the effect of the distance and tissue thickness in between.

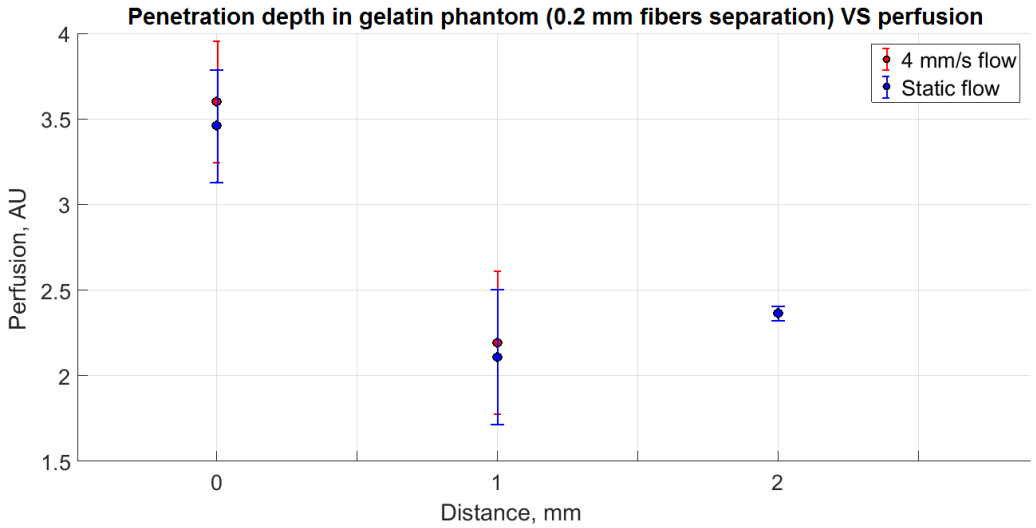

Figure 5.8: Dependence of the perfusion measurement on the laser penetration depth with 0.2 mm separation probe located inside the phantom. Blue and red markers denote the flow with 4 mm/s velocity and the static flow respectively. X axis indicates the distance between the probe and the tube in mm, while Y axis expresses the calculated perfusion in AU. The mean value of five trials with standard deviation is presented.

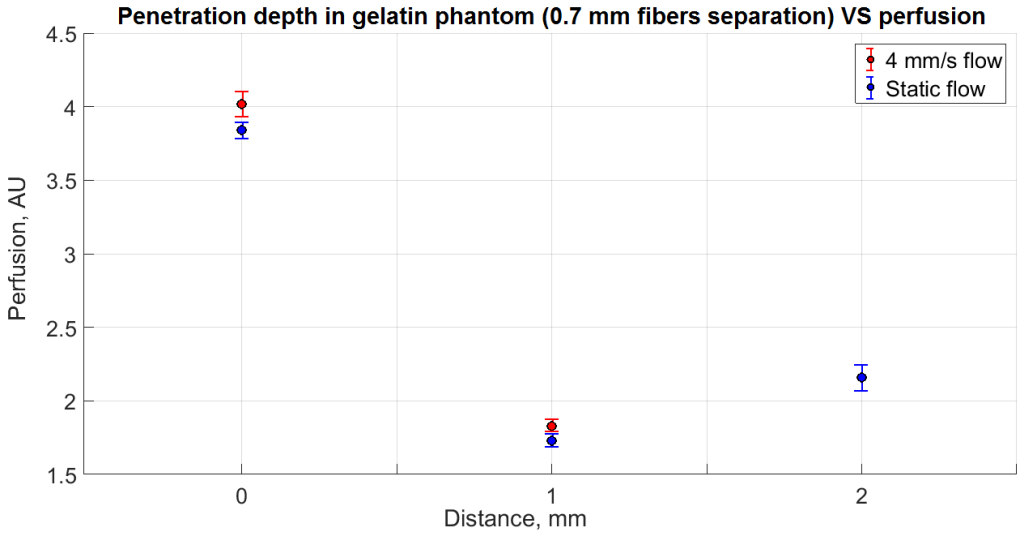

Figure 5.9: Dependence of the perfusion measurement on the laser penetration depth with 0.7 mm separation probe located inside the phantom. Blue and red markers denote the flow with 4 mm/s velocity and the static flow respectively. X axis indicates the distance between the probe and the tube in mm, while Y axis expresses the calculated perfusion in AU. The mean value of five trials with standard deviation is presented.

The maximum penetration depth, which could be achieved with created LDF system and the probes, was 1 mm. It is important to emphasize that 1 mm is a thickness of the tissue-mimicking material placed between the probe and the tube, meaning that the experiments were not performed in the air but rather in conditions, which resemble the environment of the real application. Notable degradation of the signal and some reduction of the quality of the perfusion measurement were observed when 1 mm distance was established, but determination of the flow was still possible. However, determination was not achievable at 2 mm distance between the probe and the tube. This result can be addressed to the laser attenuation phenomenon. The tissue phantom, designed in this work, has the optical properties similar to the human tissue which is highly absorbing structure. As was discussed in theoretical part, commercial laser Doppler flowmeters have the penetration depth up to 1 mm, which is similar to the demonstrated result. Moreover, increased fiber separation did not affect the measurement depth as was suggested in theory. Consequently, the created setup allows the detection of the blood vessel at maximum 1 mm distance inside the tissue before puncturing. Whether such small margin is usable in needle procedures was an open question in this

work.

An interesting observation regarding the measurement depth was made unintentionally when performing the experiments. It was noticed that if no tissue is placed between the probe and the tube, the detection distance is bigger than with tissue-mimicking material in between. Figure 5.10 demonstrates how perfusion measurement changes with the increasing distance. Perfusion could be detected even at 3 mm distance to the probe when there was nothing in between to attenuate the signal. Although such measurement situation does not refer to the real needle procedures, it was documented in case some other potential application arises.

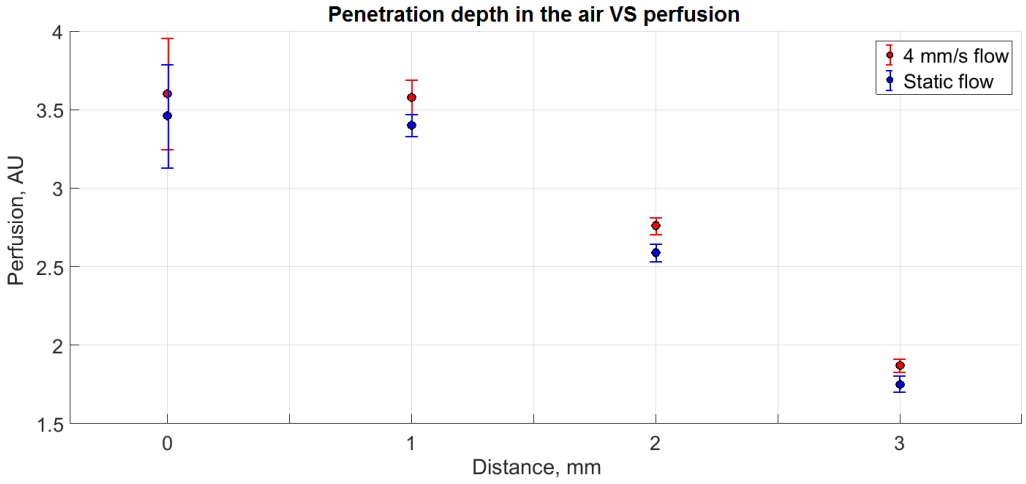

Figure 5.10: Dependence of the perfusion measurement on the measurement depth in the air. Blue and red markers denote the flow with 4 mm/s velocity and the static flow respectively. X axis indicates the distance between the probe and the tube in mm, while Y axis expresses the calculated perfusion in AU. The mean value of five trials with standard deviation is presented.

The last part of LDF measurement system evaluation was determination of the penetration angle. Figure 5.11 demonstrates the distribution of the measured perfusion at different angles between the probe and the tube. Parameters, identical to the previous experiments, were evaluated.

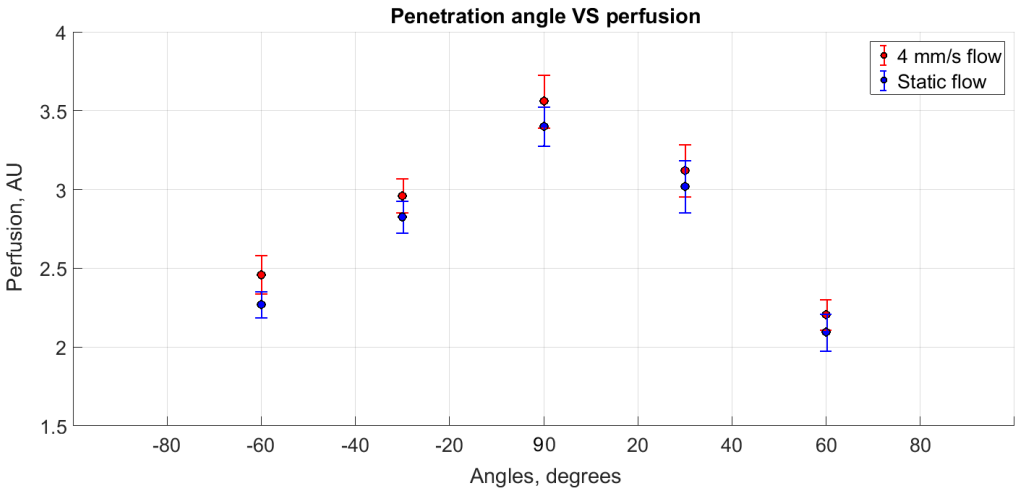

Figure 5.11: Dependence of the perfusion measurement on the laser penetration angle. Blue and red markers denote the flow with 4 mm/s velocity and the static flow respectively. X axis indicates penetration angle in degrees as was defined in section 2.3.3, while Y axis expresses the calculated perfusion in AU. The mean value of five trials with standard deviation is presented.

Apparently, the penetration angle does not have a significant effect on the quality of perfusion measurements, although the magnitude of the signal decreases when the probe moves away from the orthogonal position. This tendency is well in line with theory stating that the incident light perpendicular to the flow gives the maximum Doppler shift. Besides, no signal dependence on the flow direction was observe, which might be considered as both advantage and limitation. LDF technique lacks direction determination ability in comparison with Doppler ultrasound method, which can define the direction of the blood flow. However, the flow in big blood vessels, which are the primary targets in this work, always has a specific direction. Consequently, the direction information is unnecessary and lacking it makes the proposed system easier in design and implementation.

Figures 5.7 - 5.11 demonstrate an interesting trend of the measurements. It appeared that when the light is directed perpendicularly to the tube, penetrates entirely through the center of the flow, and the probe is in direct contact, perfusion level fluctuates from 3.5 AU to 4 AU. Partial displacement of the probe leads to a decrease of perfusion down to 2 AU - 3 AU. Finally, if perfusion cannot be measured, its level is in 1.5 AU - 2 AU range depending on the setup. These observations represent the forward problem, in which

the perfusion values are analyzed after the experiments with known variables were performed. The results were very consistent in all measurements demonstrating the potential to solve the inverse problem in which the position of the probe is defined according to the measured perfusion. However, this would require preliminary determination of the baseline, which can be the perfusion value when the probe is perfectly positioned with respect to the tube.

5.4 Measurements in tissue-mimicking environment

The purpose of the experiments with the tissue phantom was to confirm that the detection of the blood flow inside the tissue is feasible. The assumption was that the tissue-like substance would produce some constant signal due to reflections of the photons from the static scattering particles, which do not shift the signal. On the other hand, the flow located inside the substance will modify this signal due to the Doppler shift and perfusion presence when approaching the flow with the probe. The main requirement for these experiments was that they resemble the real needle procedure in order to confirm the applicability of the method in the proposed application.

Two main experiments were performed. First, the probe was approaching the tube with the flow of a certain velocity (4 mm/s) with an intention of getting in contact with the tube. Such situation simulated the case when the real medical needle is inserted into the skin towards the arteria, followed by the puncture of the blood vessel. Figure 5.12 depicts how perfusion measurement varied during this process.

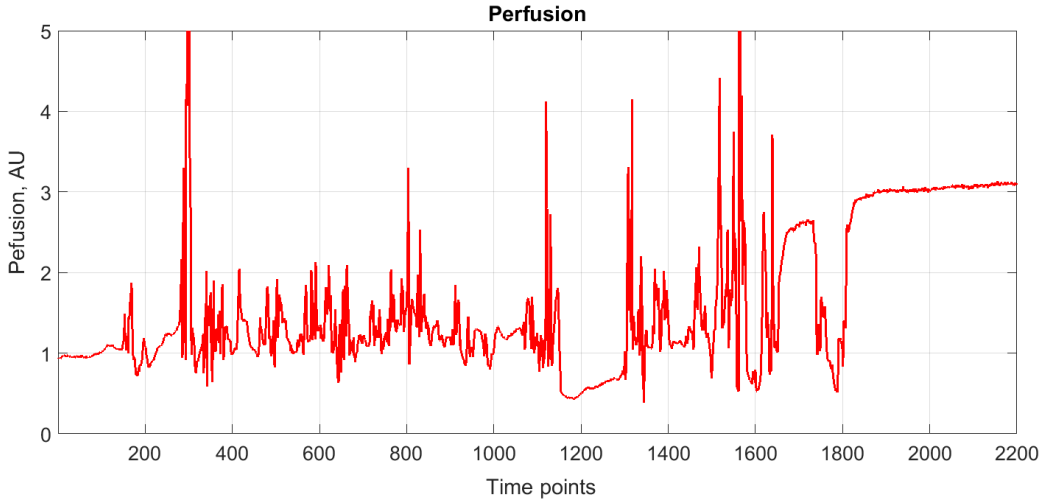

Figure 5.12: Variation of perfusion measurement when approaching the flow inside tissue-mimicking phantom. X axis indicates the time points of the measurement defined by selected segment length, while Y axis expresses the calculated perfusion in AU.

In figure 5.12 significant variations of perfusion are attributed to the noise, which is introduced when the probe slips off from the tube and the laser irradiates its walls and surrounding tissue-mimicking material instead of the flow inside the tube. When the probe is finally immobilized in place on the wall, perfusion output becomes stable. Such noisy measurements are not expected in the real tissue experiments because the needle easily punctures the wall of the blood vessel, while the same is not possible with the tube wall. In general, this experiment demonstrated that the tube, which simulates the blood vessel, can be successfully detected. However, there was a concern if the primary source of detection was the tube and not the flow inside it. Hence, further tests were performed.

The second experiment evaluated the possibility to determine the blood flow variations inside the tissue. In this case, the probe was immobilized on the tube with initially static blood flow, which was then initiated at 4 mm/s. As expected, the evident increase in perfusion value occurred demonstrating that velocity differentiation is possible not only in the air with the vessel phantom, but also inside the tissue-mimicking material. Figure 5.13 demonstrates how perfusion varied with the flow velocity.

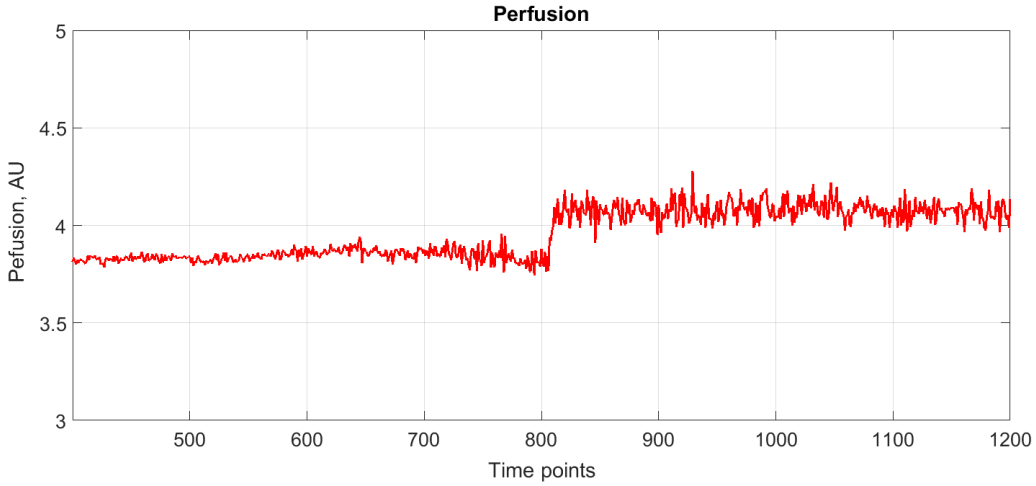

Figure 5.13: Variation of perfusion measurement with a change of the flow velocity from 0 mm/s to 4 mm/s. X axis indicates the time points of the measurement defined by selected segment length, while Y axis expresses the calculated perfusion in AU.

The experiments with the tissue phantom revealed that there is a potential to successfully detect the blood flow inside the tissue and to differentiate velocity variations when the probe is in contact with the blood vessel. However, the model is not ideal because it does not take into account the microcirculation, which would definitely introduce a certain base signal inside the tissue. In fact, as it was demonstrated in velocity evaluation experiments, the measured perfusion is small at very low velocities (below 4 mm/s), which dominate in microcirculation. Consequently, perfusion of the powerful blood flow should be detectable in spite of constantly present perfusion from the microcirculation.

5.5 Applicability, limitations and further improvements

Summarizing all the experimental results, we can conclude that created LDF system can be used in the blood vessel detection application although the particular limitations must be taken into account. It was demonstrated that the system can successfully detect different blood flow velocities in the low velocity range. It is also possible to distinguish between low and high speed

flows, thus, there is a potential to determine big blood vessels in the vicinity of the needle tip. Unfortunately, differentiation between the artery or the vein is not feasible in this case because they both have very fast blood flows and the system cannot discriminate speeds in the high velocity range due to saturation of the measurement. This is clearly the major limitation of the method for the initially proposed application.

The second limitation comes from the assessment of the penetration depth. As was demonstrated, 1 mm distance between the probe and the blood vessel with the tissue in between allows perfusion evaluation. In practice, it creates a significant risk of undesired blood vessel puncture because the needle is manipulated manually and the whole process depends on the reaction and precision of the doctor. Although the studies of the penetration angle and site demonstrated promising results, the penetration depth might be a limitation of the proposed method for the needle procedures. Nevertheless, other applications for technology, in which large measurement depth is not required, might be considered as discussed below.

The blood vessel avoidance is a crucial success factor in laparoscopic surgeries such as cholecystectomy, appendectomy and hysterectomy. Accidental cutting of big artery or vein might lead to extensive bleeding, post-surgery complications and even death of the patient. Several techniques, such as ultrasound, photoacoustic, mechanical sensors, optical coherent tomography and image processing, have already been implemented in clinical practice as the blood vessel avoidance systems with purpose to increase the level of safety during the surgery [67–71]. However, they always require insertion of additional instruments, which is inconvenient for the surgeon. The advantage of LDF method is that the optical fibers can be effectively fixed inside any surgical instrument. Besides, demonstrated limitations of LDF system should not be the restrictions for the blood vessel avoidance applications. For instance, differentiation between different speeds would become unnecessary, as any big blood vessel is the primary target. Furthermore, the requirement for the penetration depth would not be high because the probe configuration is not restricted to the needle anymore. Consequently, the system can be implemented as the blood vessel avoidance improvement for laparoscopic surgeries without significant modifications.

One hardware improvement, which was not investigated in this work, should still be implemented and evaluated. The laser operation mode is a parameter, which might affect the laser penetration depth. In the setup described in this work, the continuous wave laser mode was used, while some researchers demonstrated that the pulsed mode might have an effect on the depth of laser penetration through the tissue [43, 72]. Such response to the laser pulsing occurs because the generated pulses have much higher energy

than the continuous wave laser, even though the impact lasts only several milliseconds. Therefore, the attenuation of the laser by means of absorption occurs deeper inside the skin. The necessary energy of the pulse and power of the laser must be defined experimentally, because the laser must not burn the skin, and there is no predefined guideline at which laser power it occurs. No experiments with real tissue and the pulsed laser were carried out before, thus the result of such improvement is questionable. This potential enhancement was not investigated because it required additional hardware, which was not realized during this work.

Finally, in order to make a conclusion regarding the system applicability, animal experiments are required. The measurement in the living tissue is the only reliable way to assess the effectiveness of the presented device and technology. Nevertheless, animal studies are expensive and can be performed only with special approvals, which are difficult to obtain. Consequently, before moving to this step it is necessary to evaluate all presented results and determine if revealed limitations restrict the application field dramatically or the technique still has a potential for some medical area.

Chapter 6

Conclusion

In this work, a novel system for medical procedures based on laser Doppler flowmetry technology was designed, constructed and evaluated. Initially, a proposed application area for created system was the medical needle procedures, although LDF had not been utilized in such practice before. Consequently, the work involved thorough theoretical study of previously performed LDF research with further assessment of its applicability in the proposed application. According to theory, the measurement setup was constructed. The performance and capabilities of the system were assessed based on the experimental results. The research questions, which were raised in the beginning, were considered and the answers were provided.

Conventionally, LDF technology is used in microcirculation measurements, in which the blood perfusion is very small. Nevertheless, it was successfully demonstrated that developed system can detect much more significant perfusion and differentiate between the flows with high and low velocities. An operation range of the system was evaluated in respect to the various penetration angles, depths and sites. The system could effectively determine the blood flow when the laser penetrated the experimental tube in the center or partially through the wall. Moreover, the measurement was achievable at 3 mm distance between the probe and the tube in the air and at 1 mm distance inside the phantom. Perfusion was defined at any penetration angle with condition that the laser beam irradiated the flow. Final experiments revealed that the flow can be detected in tissue-mimicking phantom meaning that the method has a potential for the needle procedures.

The characterization experiments revealed several limitations of the described method. Although the penetration angle and the puncturing site could be varied, the penetration depth was very limited. The distance of 1 mm between the probe and the blood vessel is a small and unsafe margin in the needle insertion procedures. Additionally, the restriction of the flow

velocity determination was discovered. The velocities could not be separated if they were much higher that 8 mm/s. Thus, the system cannot reliably distinguish between the arteria and the vein. This might be a limitation for the catheter installation procedures where precise puncturing is desired, however, other medical interventions can be effectively improved with the proposed technology.

Even through the developed LDF system features apparent limitations, technology is potentially applicable in the medical needle procedures after a number of challenges is addressed. In particular, further work on hardware improvements and additional experimental trials are required. Furthermore, the experimental results demonstrated that certain medical interventions, in which contact with the blood vessels must be avoided, can benefit from developed LDF setup. Among such interventions are laparoscopic surgery or the needle procedures that target the cancerous tissue (biopsies) or the epidural space. The proposed system would be a valuable enhancement of the existing medical techniques due to its simplicity and straightforward integration into conventional tools and equipment.

References

[1] Surgical procedures (shortlist): Mapping with ICD-9-CM oecd/eurostat/who-europe joint data collection on non-monetary health care statistics, 2007. Accessed: 2016-04-10.

[2] Catheter Angiography RadiologyInfo. `https://www.radiologyinfo.org/en/info.cfm?pg=angiocath`. Accessed: 2016-02-16.

[3] Tanimoto, M., Arai, F., Fukuda, T., Iwata, H., Itoigawa, K., Gotoh, Y., Hashimoto, M., and Negoro, M. Micro force sensor for intravascular neurosurgery. *Proceedings of International Conference on Robotics and Automation 2* (1997), 1561–1566.

[4] Baker, D. W. Pulsed ultrasonic Doppler blood-flow sensing. *IEEE Transactions on Sonics and Ultrasonics 17*, 3 (1970), 170–184.

[5] Sigel, B., Felix, W. R., Popky, G. L., and Ipsen, J. Diagnosis of lower limb venous thrombosis by Doppler ultrasound technique. *Archives of Surgery 104*, 2 (1972), 174–179.

[6] Ultrasound Therapy Breaks Up Blood Clots . `https://www.nibib.nih.gov/news-events/newsroom/ultrasound-therapy-breaks-blood-clots`. Accessed: 2016-01-15.

[7] Needling Techniques Obstetric Anesthesia. `http://pie.med.utoronto.ca/OBAnesthesia/OBAnesthesia_content/OBA_needling_module.html`. Accessed: 2016-02-22.

[8] Branched 4 Vessel Ultrasound Training Block Model CAE Heathcare. `http://www.bluephantom.com/details.aspx?cid=&pid=64`. Accessed: 2016-03-25.

[9] Riva, C., Ross, B., and Benedek, G. B. Laser Doppler measurements of blood flow in capillary tubes and retinal arteries. *Investigative Ophthalmology & Visual Science 11*, 11 (1972), 936–944.

[10] PeriFlux System 5000 Perimed AB. `https://www.perimed-instruments.com/products/periflux-system-5000-ldpm`. Accessed: 2016-12-20.

[11] Laser Doppler Monitor moorVMS-LDF Moor Instruments. `https://gb.moor.co.uk/product/moorvms-ldf-laser-doppler-monitor/1`. Accessed: 2016-12-20.

[12] Brochure PeriFlux System 5000 Perimed AB. Accessed: 2016-12-20.

[13] Fredriksson, I. *Quantitative laser Doppler flowmetry*. PhD thesis, Linköping University Electronic Press, 2009.

[14] Stern, M. In vivo evaluation of microcirculation by coherent light scattering.

[15] Bonner, R., and Nossal, R. Model for laser Doppler measurements of blood flow in tissue. *Applied Optics 20*, 12 (1981), 2097–2107.

[16] Jentink, H., De Mul, F., Hermsen, R., Graaff, R., and Greve, J. Monte carlo simulations of laser doppler blood flow measurements in tissue. *Applied Optics 29*, 16 (1990), 2371–2381.

[17] Larsson, O. Digital Implementation of a Laser Doppler Perfusion Monitor, 2006.

[18] Leahy, M., Liebert, A., and Maniewski, R. Evaluation of different signal processing algorithms in laser Doppler perfusion measurements. In *OPTO Ireland* (2003), International Society for Optics and Photonics, pp. 120–127.

[19] Nilsson, G., Jakobsson, A., and Wardell, K. Imaging of tissue blood flow by coherent light scattering. In *Engineering in Medicine and Biology Society, 1989. Images of the Twenty-First Century., Proceedings of the Annual International Conference of the IEEE Engineering in* (1989), IEEE, pp. 391–392.

[20] Nilsson, G., Salerud, G., Strömberg, T., Wårdell, K., and Larsson, M. Laser Doppler perfusion monitoring and imaging.

[21] Briers, J. D. Laser doppler, speckle and related techniques for blood perfusion mapping and imaging. *Physiological Measurement 22*, 4 (2001), R35.

[22] Kiyokura, T., Mino, S., and Shimada, J. Wearable laser blood flowmeter. *NTT Technical Review 1* (2006), 38–43.

[23] Kimura, Y., Goma, M., Onoe, A., Higurashi, E., and Sawada, R. Integrated laser Doppler blood flowmeter designed to enable wafer-level packaging. *IEEE Transactions on Biomedical Engineering 57*, 8 (2010), 2026–2033.

[24] Kuwabara, K., Higuchi, Y., Ogasawara, T., Koizumi, H., and Haga, T. Wearable blood flowmeter appcessory with low-power laser Doppler signal processing for daily-life healthcare monitoring. In *Engineering in Medicine and Biology Society (EMBC), 2014 36th Annual International Conference of the IEEE* (2014), IEEE, pp. 6274–6277.

[25] Shepherd, A. P., and Öberg, P. Å. *Laser-Doppler blood flowmetry*, vol. 107. Springer Science & Business Media, 2013.

[26] Fredriksson, I., Fors, C., and Johansson, J. Laser doppler flowmetry-a theoretical framework. *Department of Biomedical Engineering, Linköping University* (2007), 6–7.

[27] Leahy, M., De Mul, F., Nilsson, G., and Maniewski, R. Principles and practice of the laser-Doppler perfusion technique. *Technology and Health Care 7*, 2-3 (1999), 143–162.

[28] Serov, A. N. *Novel instruments for remote and direct-contact laser Doppler Perfusion imaging and monitoring.* 2002.

[29] Jonasson, H. *Model-based quantitative assessment of skin microcirculatory blood flow and oxygen saturation.* PhD thesis, Linköping University Electronic Press, 2016.

[30] Fredriksson, I., Larsson, M., Strömberg, T., et al. Absolute flow velocity components in laser Doppler flowmetry. In *Proc. SPIE* (2006), vol. 6094, p. 60940A.

[31] Nilsson, G. Signal processor for laser Doppler tissue flowmeters. *Medical and Biological Engineering and Computing 22*, 4 (1984), 343–348.

[32] Liebert, A., Leahy, M., and Maniewski, R. A calibration standard for laser-Doppler perfusion measurements. *Review of Scientific Instruments 66*, 11 (1995), 5169–5173.

[33] Figueiras, E., Campos, R., Semedo, S., Oliveira, R., Requicha Ferreira, L., and Humeau-Heurtier, A. A new laser Doppler flowmeter prototype for depth dependent monitoring of skin microcirculation. *Review of Scientific Instruments 83*, 3 (2012), 034302.

[34] Figueiras, E. M. A. *Métodos de instrumentação para fluxometria laser: aplicações à microcirculação sanguínea*. PhD thesis, 2012.

[35] Liebert, A., Leahy, M., and Maniewski, R. Multichannel laser-Doppler probe for blood perfusion measurements with depth discrimination. *Medical and Biological Engineering and Computing 36*, 6 (1998), 740–747.

[36] Figueiras, E., Oliveira, R., Lourenço, C. F., Campos, R., Humeau-Heurtier, A., Barbosa, R. M., Laranjinha, J., Ferreira, L. F. R., and de Mul, F. F. Self-mixing microprobe for monitoring microvascular perfusion in rat brain. *Medical & Biological Engineering & Computing 51*, 1-2 (2013), 103–112.

[37] Boggett, D., Blond, J., and Rolfe, P. Laser Doppler measurements of blood flow in skin tissue. *Journal of Biomedical Engineering 7*, 3 (1985), 225–232.

[38] Olshausen, B. A. Aliasing. *PSC 129–Sensory Processes* (2000), 3–4.

[39] Fredriksson, I., Larsson, M., and Strömberg, T. Model-based quantitative laser Doppler flowmetry in skin. *Journal of Biomedical Optics 15*, 5 (2010), 057002–057002.

[40] Clough, G., Chipperfield, A., Byrne, C., de Mul, F., and Gush, R. Evaluation of a new high power, wide separation laser doppler probe: potential measurement of deeper tissue blood flow. *Microvascular Research 78*, 2 (2009), 155–161.

[41] Lohwasser, R., and Soelkner, G. Experimental and theoretical laser-doppler frequency spectra of a tissuelike model of a human head with capillaries. *Applied Optics 38*, 10 (1999), 2128–2137.

[42] Laser Doppler probes Perimed AB . `https://www.perimed-instruments.com/upl/files/103718`. Accessed: 2016-01-15.

[43] Steenbergen, W., Kolkman, R. G., Woldberg, S., and de Mul, F. F. Pulsed laser Doppler flowmetry for increased signal-to-noise ratio and probed depth. In *Biomedical Optics 2003* (2003), International Society for Optics and Photonics, pp. 49–54.

[44] Soelkner, G., Mitic, G., and Lohwasser, R. Monte Carlo simulations and laser Doppler flow measurements with high penetration depth in biological tissuelike head phantoms. *Applied Optics 36*, 22 (1997), 5647–5654.

[45] Photodiode/Phototransistor Application Circuit Sharp Application Note. `http://physlab.org/wp-content/uploads/2016/03/Photodiode_circuit.pdf`. Accessed: 2016-02-16.

[46] Morales, F. *Improving the clinical applicability of laser Doppler perfusion monitoring*. University Library Groningen][Host], 2005.

[47] Larsson, M., and Strömberg, T. Toward a velocity-resolved microvascular blood flow measure by decomposition of the laser Doppler spectrum. *Journal of Biomedical Optics 11*, 1 (2006), 014024–014024.

[48] Kenneth, S. S., and Carol, M. Anatomy and physiology: The unity of form and function, 1998.

[49] Bashkatov, A., Genina, E., Kochubey, V., and Tuchin, V. Optical properties of human skin, subcutaneous and mucous tissues in the wavelength range from 400 to 2000 nm. *Journal of Physics D: Applied Physics 38*, 15 (2005), 2543.

[50] Hemoglobin undergraduate course at Davidson College. `http://www.bio.davidson.edu/Courses/Molbio/MolStudents/spring2005/Heiner/hemoglobin.html`. Accessed: 2016-12-22.

[51] Ambardekar, A. V., Hunter, K. S., Babu, A. N., Tuder, R. M., Dodson, R. B., and Lindenfeld, J. Changes in aortic wall structure, composition, and stiffness with continuous-flow left ventricular assist devicesclinical perspective. *Circulation: Heart Failure 8*, 5 (2015), 944–952.

[52] Tuchin, V. V. Tissue optics: tomography and topography. In *Saratov Fall Meeting'98: Light Scattering Technologies for Mechanics, Biomedicine, and Material Science* (1999), International Society for Optics and Photonics, pp. 168–198.

[53] Niemz, M. H. *Laser-tissue interactions: fundamentals and applications*. Springer Science & Business Media, 2013.

[54] Fredriksson, I., Larsson, M., and Strömberg, T. Optical microcirculatory skin model: assessed by Monte Carlo simulations paired

with in vivo laser Doppler flowmetry. *Journal of Biomedical Optics 13*, 1 (2008), 014015–014015.

[55] Salomatina, E., Jiang, B., Novak, J., and Yaroslavsky, A. N. Optical properties of normal and cancerous human skin in the visible and near-infrared spectral range. *Journal of Biomedical Optics 11*, 6 (2006), 064026–064026.

[56] Jacques, S. Skin Optics. Oregon medical laser center news, 1998.

[57] Huang, Y.-Y., Chen, A. C.-H., and Hamblin, M. Low-level laser therapy: an emerging clinical paradigm. *SPIE Newsroom 9* (2009), 1–3.

[58] Roggan, A., Friebel, M., Dörschel, K., Hahn, A., and Muller, G. Optical properties of circulating human blood in the wavelength range 400-2500 nm. *Journal of Biomedical Optics 4*, 1 (1999), 36–46.

[59] Friebel, M., Roggan, A., Müller, G., and Meinke, M. Determination of optical properties of human blood in the spectral range 250to1100nm using Monte Carlo simulations with hematocrit-dependent effective scattering phase functions. *Journal of Biomedical Optics 11*, 3 (2006), 034021–034021.

[60] Jacques, S., and Prahl, S. Absorption spectra for biological tissues (oregon medical laser center, or).

[61] Richards-Kortum, R., and Sevick-Muraca, E. Quantitative optical spectroscopy for tissue diagnosis. *Annual Review of Physical Chemistry 47*, 1 (1996), 555–606.

[62] Near/Short Wave Infrared Sensors for High Resolution Imaging in Tissue Sensors Unlimited. `http://www.sensorsinc.com/applications/medical/imaging-tissue-in-swir`. Accessed: 2016-02-14.

[63] Qin, J., and Lu, R. Measurement of the absorption and scattering properties of turbid liquid foods using hyperspectral imaging. *Applied Spectroscopy 61*, 4 (2007), 388–396.

[64] Michalski, M.-C., Briard, V., and Michel, F. Optical parameters of milk fat globules for laser light scattering measurements. *Le Lait 81*, 6 (2001), 787–796.

[65] Pogue, B. W., and Patterson, M. S. Review of tissue simulating phantoms for optical spectroscopy, imaging and dosimetry. *Journal of Biomedical Optics 11*, 4 (2006), 041102–041102.

[66] Syringe Needle Gauge Chart Sigma-Aldrich. `http://www.sigmaaldrich.com/chemistry/stockroom-reagents/learning-center/technical-library/needle-gauge-chart.html`. Accessed: 2016-01-30.

[67] Ohdaira, T., and Nagai, H. A vertical scanning Doppler probe identifies blood vessels during laparoscopic surgery. *Surgical Endoscopy 21*, 5 (2007), 782–784.

[68] Horstmann, J., Baade, A., and Brinkmann, R. Photoacoustic blood vessel detection during surgical laser interventions. In *European Conference on Biomedical Optics* (2011), Optical Society of America, p. 80920Z.

[69] Glavi, Z., Begi, L., and Rozman, R. A new device for the detection and recognition of blood vessels in laparoscopic surgery. *Surgical Endoscopy 16*, 8 (2002), 1197–1200.

[70] Liang, C.-P., Wu, Y., Schmitt, J., Bigeleisen, P. E., Slavin, J., Jafri, M. S., Tang, C.-M., and Chen, Y. Coherence-gated Doppler: a fiber sensor for precise localization of blood flow. *Biomedical Optics Express 4*, 5 (2013), 760–771.

[71] Akbari, H., Kosugi, Y., and Kihara, K. A novel method for artery detection in laparoscopic surgery. *Surgical Endoscopy 22*, 7 (2008), 1672–1677.

[72] Kolkman, R. G. M. *Photoacoustic & pulsed laser-doppler monitoring of blood concentration and perfusion in tissue*. PhD thesis, University of Twente, 2002.